Journal of Medicinal Chemistry

Article

Bioactivatable pseudo-tripeptidization of cyclic dipeptides to increase the affinity toward oligopeptide transporter 1 for enhanced oral absorption: an application to cyclo(L-Hyp-L-Ser) (JBP485)

Qikun Jiang, Jiangnan Zhang, Peiyue Tong, Yan Gao, Yiqin Lv, Changyuan Wang, Meiling Luo, Mengchi Sun, Jian Wang, Yao Feng, Linlin Cao, Gang Wang, Yang Wang, Qiming Kan, Tianhong Zhang, Yongjun Wang, Kexin Liu, Jin Sun, and Zhonggui He

J. Med. Chem., **Just Accepted Manuscript** • DOI: 10.1021/acs.jmedchem.9b00358 • Publication Date (Web): 08 Aug 2019

Bioactivatable pseudo-tripeptidization of cyclic dipeptides to increase the affinity toward oligopeptide transporter 1 for enhanced oral absorption: an application to cyclo(L-Hyp-L-Ser) (JBP485)

Qikun Jiang,[a] Jiangnan Zhang,[f] Peiyue Tong,[a] Yan Gao,[a] Yiqin Lv, [a] Changyuan Wang,[f] Meiling Luo,[a] Mengchi Sun,[a] Jian Wang,[b] Yao Feng,[b] Linlin Cao,[c] Gang Wang,[d] Yang Wang,[d] Qiming Kan,[e] Tianhong Zhang,[a] Yongjun Wang,[a] Kexin Liu,[f] Jin Sun,[*,a] Zhonggui He[*,a]

[a] Department of Pharmaceutics, Wuya College of Innovation, Shenyang Pharmaceutical University, Shenyang 110016, China

[b] Key Laboratory of Structure-Based Drug Design and Discovery, Shenyang Pharmaceutical University, Ministry of Education, Shenyang 110016, China

[c] Department of Pharmaceutics, The Second Hospital of Dalian Medical University, Dalian 116023, China

[d] Department of Pharmaceutics, Guang Xi University of Chinese Medicine, Guangxi 530001, China

[e] Department of Pharmacology, Shenyang Pharmaceutical University, Shenyang 110016, China

[f] Department of Clinical Pharmacology, Dalian Medical University, Dalian 116044, China

ABSTRACT

The cyclic dipeptides generally present lower affinity toward intestinal oligopeptide transporter 1 (PEPT1) than the linear dipeptides. JBP485 (cyclo(L-Hyp-L-Ser)) is a low-affinity substrate of PEPT1 with poor oral bioavailability. However, JBP923 (L-Hyp-L-Ser) is a high-affinity substrate of PEPT1 with high oral absorption. We hypothesize that the bioactivatable pseudo-tripeptidization prodrug strategy is promising to increase the affinity of cyclic dipeptides toward PEPT1. To test our hypothesis, we design five amino acid ester prodrugs of JBP485. Compared with JBP485, the optimal prodrug (JBP485-3-CH_2-O-valine, J3V) demonstrates improved affinity of PEPT1, oral bioavailability in rats and beagle dogs. Moreover, J3V can dose-dependently protect against liver injury. Additionally, J3V is stable in the gastrointestinal tract, beneficial to the PEPT1-medited membrane transport, and is bioactivated in the enterocytes and hepatic cells, essential to elicit its bioactivity. In summary, the bioactivatable pseudo-tripeptidization strategy shows potential in increasing affinity of PEPT1 to enhance oral bioavailability of cyclic dipeptides.

KEYWORDS: bioactivatable pseudo-tripeptidization, cyclic dipeptides, linear dipeptides, JBP485

INTRODUCTION

Cyclic dipeptides are heterocyclic compounds comprising of two amino acid residues linked to a central diketopiperazine (DPK) ring structure, and have various biological activities such as anti-inflammatory[1], anti-microbial[2], anti-diabetic activity[3]. However, it had been reported that the intestinal permeability of some cyclic dipeptides was lower than that of its counterpart, the linear dipeptides[4, 5]. Most linear dipeptides could be actively transported by oligopeptide transporter 1 (PEPT1, *SLC15A1*), which is highly expressed in the apical membrane of enterocytes[6], whereas the cyclic dipeptides generally present lower affinity toward PEPT1 than the linear dipeptides[7], even not recognised by PEPT1[8, 9]. The reason for low affinity of PEPT1 for cyclic dipeptides is that the key pharmacophores of linear dipeptides responsible for interacting with PEPT1 were masked after cyclization, such as *C*-terminal carboxylic or N-terminal amino group of linear dipeptides[6, 10]. Several formulation approaches have been attempted previously to increase the bioavailability of cyclic dipeptides, including the preparation of PLGA-based nanoparticles[11] or emulsions[12]. However, these strategies have some limitations, such as complex preparation process[13],low drug loading[14] and unfavourable stability[15]. Until now, no prodrug approach has been adopted to improve the oral bioavailability of cyclic dipeptides.

In recent years, the understanding of membrane transporters in the intestine has prompted a novel transporter-targeted prodrug approach to overcome the poor membrane permeability[16]. Since PEPT1 could mediate the transport of dipeptides, tripeptides and various of peptidomimetics, the broad substrate specificity of PEPT1 makes it an attractive target for designing oral prodrugs[10]. The PEPT1-mediated prodrug approach is effective in increasing intestinal permeability and oral absorption, using amino acids as targeting promoieties[17]. Most amino acid prodrugs are classified as amide- and ester-type prodrugs, in which α-carboxylic or α-amine group of amino acids is conjugated with functional groups of the parent compounds (hydroxyl, amine, and carboxyl)[18], respectively. The amino acid ester prodrugs are preferred for designing PEPT1-targeted prodrugs, because they show reasonably good stability

over the gastrointestinal pH range and simultaneously maintain a rapid rate of enzymatic-mediated bioactivation. For examples, valganciclovir, the valine ester prodrugs of poorly absorbed nucleoside analogue antiviral drug-ganciclovir, exhibited good oral absorption[19]. This PEPT1-mediated prodrug approach was also successfully applied to other poorly absorbed nucleosides by our group to increase oral absorption[20-22].

Inspired by the above findings, we hypothesize that the pseudo-tripeptidization strategy, amino acid ester prodrugs of cyclic dipeptides, could increase the binding affinity of PEPT1. Our assumption is stated as follows: firstly, since the PEPT1 recognition is influenced by peptide size, the amino acid esters of cyclic dipeptides, the size of which is similar to tripeptides, would be accommodated by the binding pocket of PEPT1; secondly, the N-terminal amino group of amino acids introduced into the prodrugs would facilitate interaction with PEPT1. Furthermore, according to the chemical/enzymatic stability of amino acid ester prodrugs, we proposed that the high chemical stability would reduce the conversion of the amino acid ester prodrugs of cyclic dipeptides prior to absorption in the gastrointestinal (GI) tract, whereas bioactivation by multiple enzymes in the enterocytes and hepatic cells could allow for quick and quantitative conversion to the active parent molecule.

JBP485 (cyclo(L-Hyp-L-Ser), Figure 1A) and JBP923 (L-Hyp-L-Ser, Figure 1B) are firstly isolated from hydrolysate of human placenta (Laennec®) and used to treat anti-hepatitis and anti-aging[23, 24]. The activity of JBP485 is notably higher than that of JBP923 at the same dose after intravenous administration[25]. However, JBP485 has a weaker potency after oral administration, due to the low oral bioavailability (about 20%) for JBP485, but JBP923 is nearly 100% absorbed[25, 26]. It had been reported that JBP485 and JBP923 were actively transported by PEPT1. However, the PEPT1 affinity of JBP923 was higher than that of JBP485, with inhibition constant (K_i) for JBP485 and JBP923 in relation to the uptake of Gly-Sar being 36.0 and 2.5 mM, respectively[5]. The low binding affinity of JBP485 toward PEPT1 was responsible for low oral bioavailability of JBP485.

Herein, we put forward the bioactivatable pseudo-tripeptidization strategy to

increase the PEPT1 affinity of JBP485. We had synthesized five amino acid ester prodrugs of JBP485 (Figure 1(C-G)). These prodrugs were screened regarding the chemical/metabolic stability study, cellular permeation in the Caco-2 cell monolayers and oral pharmacokinetic study in rats and beagle dogs. These results demonstrated that the optimal prodrug (JBP485-3-CH_2-O-Valine, J3V) was stable in the gastrointestinal tract of rats and then was bioactivated by multiple activating enzymes in the intestine and liver of rats. J3V exhibited significantly high bioavailability compared to JBP485 after oral administration in rats and beagle dogs, due to the high PEPT1 affinity of J3V.

RESULTS AND DISCUSSION

Design and synthesis of JBP485 and its prodrugs

To increase the binding affinity of PEPT1 for JBP485, five amino acid prodrugs (JBP485-3-CH_2-O-Valine (J3V), JBP485-3-CH_2-O-Leucine (J3L), JBP485-3-CH_2-O-Isoleucine (J3I), JBP485-3-CH_2-O-Phenylalanine (J3P), JBP485-7-O-Valine (J7V)) were synthesized according to the synthetic procedures (Figure 2). Firstly, four prodrugs (J3V, J3L, J3I, J3P) were synthesized by conjugating the low steric hindrance 3-methyl-hydroxyl of JBP485 with the series of the carboxyl groups of amino acids (L-valine, L-leucine, L-isoleucine, L-phenylalanine) to investigate the effects of amino acid promoieties on the PEPT1 affinity; secondly, compared to J3V, J7V was designed to study the steric hindrance effect of ester bond on the affinity for PEPT1. JBP485 and its prodrugs were fully characterized by HPLC, H^1 NMR, and HRMS. Detailed synthetic procedures, yields, and HPLC purity were given in the experimental sections.

Stability Study

Chemical stability

To target effectively the PEPT1 transporter in the apical side of enterocytes, the prodrugs should be stable in the GI tract prior to intestinal membrane transport. The chemical stability was examined over the gastrointestinal pH range (0.1M HCl, pH

4.5 acetate buffer, pH 5.8 phosphate buffer, pH 6.8 phosphate buffer and pH 7.2 phosphate buffer). As shown in Table 1, JBP485 was less susceptible to different pH changes, demonstrating that JBP485 was stable in the GI tract. The stability for all prodrugs increased with decreasing pH and followed the rank order of J3I>J7V>J3V>J3P=J3L. In addition, the $t_{1/2}$ values in the simulated gastric/intestinal fluids were similar to those in 0.1 M HCl and pH 6.8 phosphate buffer, demonstrating that all prodrugs were not hydrolyzed by pepsin and trypsin in the GI tract. The $t_{1/2}$ values of J3V, J7V and J3I was 7.9-20.0 h in the simulated gastric/intestinal fluids, indicating that these prodrugs could ensure sufficient stability during the transport process in the intestine. However, J3P and J3L could be instable in the intestine because of short $t_{1/2}$ values in the simulated intestinal fluids.

Metabolic stability

Except for chemical stability, metabolic stability of prodrugs was investigated in rat jejunum and liver homogenates and plasma (Table 1). The metabolic stability study provided the bioactivation performances of prodrugs to JBP485 in these metabolic sites after oral administration. The $t_{1/2}$ was >20 h for JBP485 in jejunum and liver homogenate and plasma, thus excluding the possibilities that low bioavailability of JBP485 was mainly due to instability in these metabolic sites. This was also consistent with the previous results that the first-pass hepatic metabolism of JBP485 could be neglected because its bioavailability after port vein injection was 85% [26]. Additionally, the rank order in metabolic stability of all prodrugs was the same as those in chemical stability. The $t_{1/2}$ in tissue homogenates and plasma were 3-35-fold shorter than that in pH 7.4 phosphate buffer, indicating the enzyme-catalyzed hydrolysis for all prodrugs in tissues. Moreover, the $t_{1/2}$ values of all prodrugs in the jejunum and liver homogenates were shorter than that in the plasma, implying that the primary bioactivation sites of prodrugs might be the liver and intestine.

Caco-2 Membrane Permeability

The permeability of JBP485 and its prodrugs across Caco-2 cell monolayers was

shown in Figure 3A. The amino acid prodrugs (J3V, J3I, J7V) showed 2.4-11.6-fold increase in permeability compared to JBP485, while J3L and J3P didn't increase the permeability. J3V showed the highest permeability and was nearly similar to JBP923, a known substrate of PEPT1 with up to 100% oral bioavailability in rats. Consequently, J3V was chosen for further study to investigate the single-pass intestinal perfusion study, cellular uptake study, oral pharmacokinetics and antihepatitis activity.

Correlation of lipophilicity and permeability

The pH-dependent distribution coefficient (log D), predicted by Discovery Studio 3.5 Client software, was the principal parameter to estimate lipophilicity of chemical compound. Figure 3B showed the correlation between Caco-2 membrane permeability and lipophilicity. JBP923 had the lowest log D value and JBP485 and its prodrugs had similar log D values. However, lipophilicity was not correlated with the high Caco-2 membrane permeability of JBP923 and J3V, indicating that a different permeation pathway than passive diffusion is responsible for the high permeability of JBP923 and J3V.

Single-pass intestinal perfusion (SPIP) study in rats

The effective permeability (P_{eff}) of JBP485, J3V and JBP923 were determined using the in situ single-pass intestinal perfusion system in rats. As shown in Figure 3C, JBP485 had low permeability in the jejunum, consistent well with the low permeability in Caco-2 cell monolayers. However, the permeability of J3V was similar to JBP923, and was 6.03-fold higher than JBP485. To investigate whether the increased intestinal permeability of J3V was due to improved affinity toward PEPT1, an inhibition study was performed by co-perfusing three compounds (JBP485, JBP923, J3V) with Gly-Sar (the well-known and non-metabolized PEPT1 substrate), respectively. The P_{eff} values of JBP485, J3V and JBP923 in the presence of Gly-Sar were reduced by 2.5-, 6.8-, 7.3-fold, respectively, demonstrating that JBP485, J3V and JBP923 were the typical substrates of PEPT1 and the affinity of J3V was higher

than that of JBP485.

Cellular uptake mechanism of JBP485 and J3V

The SPIP study strongly suggested that JBP485, J3V and JBP923 were PEPT1 substrates and the PEPT1 affinity of J3V was the highest. To further verify these findings, the cellular uptake mechanism of J3V and JBP485 in the Caco-2 cells was investigated, with JBP923 as a positive control. The PEPT1 transporter is driven by an inwardly-directed proton gradient which catalyzes the co-transport of the substrates. As shown in Figure 4A, J3V and JBP923 showed an approximate 1.7-2.5-fold increase in cellular uptake compared to JBP485 at pH 6.0. However, the cellular uptake amounts of JBP485, J3V and JBP923 were significantly decreased when changing pH from 6.0 to 7.4 or co-perfusing with 50 mM Gly-Sar at pH 6.0 (Figure 4A-4B), respectively. These results were consistent with the results of SPIP study, further confirming that these compounds were substrates of PEPT1.

Since other transporters, such as OATP-B (SLC *21A9*), OCT1 (SLC *22A1*) and OCT3 (SLC *22A3*), could be involved in the peptides transport through small intestine wall, the inhibition kinetic assay of OATP-B and OCTs (OCT1 and OCT3) substrates in Caco-2 cells was also evaluated in order to confirm whether JBP485 and J3V had interacted with these transporters. Figure 4C indicated that J3V and JBP485 showed no significant difference in cellular uptake in the presence or absence of captopril (substrates of OATP-B) and metformin (substrates of OCT1-3), demonstrating that JBP485 and J3V were not considered to be the substrates of OATP-B and OCTs.

We further compared the PEPT1 affinity of JBP485, J3V and JBP923, using the saturable transport and Gly-Sar inhibition kinetic assays in Caco-2 cells. Kinetic analysis showed that the K_m value of J3V was roughly 3.0-fold lower than that of JBP485, which compared favorably to JBP923 (Figure 5A-5C, Table 2). Additionally, the IC_{50} values for JBP485, J3V and JBP923 to inhibit Gly-Sar uptake in Caco-2 cells were listed from the curves (Figure 5D, Table 2). The rank order of IC_{50} values of these compounds against the Gly-Sar uptake was similar to the rank order of K_m values of the saturable kinetics. The J3V and JBP923 showed the highest inhibition

effects on Gly-Sar uptake, with IC_{50} values being 2.9, 1.76 and 18.2 mM, respectively, which demonstrated that J3V and JBP923 showed 6.3-10.3-fold improvement in affinity over JBP485.

Molecular docking

The crystal structure of the hPEPT1 protein has not been resolved, and so we chose a homology modeling of hPEPT1. To date, bacterial peptide transporters have been proven to be valid and reliable model system contributing to understand the molecular basis of peptide recognition within hPEPT1 transporters. We selected the $PEPT_{so}$ with high degree of sequence conservation within the transmembrane (TM) region (35% identity) as PEPT1 proteins. The Glu595 and Arg34 were the two important conserved residues on the substrate-binding sites of $PEPT_{so}$[27, 28]. The interaction profiles of the homology model with these ligands (JBP485, J3V and JBP923) were illustrated in Figure 6. These ligands interacted with the key substrate-binding site residues (Glu595, Arg34) of $PEPT_{so}$, demonstrating that these ligands could be recognised via the $PEPT_{so}$. However, around 1.3-fold and 1.5-fold increase in binding energy scores obtained from -4.8 up to -6.4 and -7.2 kcal/mol for JBP485, J3V and JBP923, respectively. These indicated that stronger binding of J3V and JBP923 with $PEPT_{so}$ would favor its transportation in comparison with JBP485. These findings were consistent with the above results of cellular permeability and uptake study. This discrepancy for the PEPT1 affinity of these ligands was due to the difference of bond strength between these ligands (JBP485, J3V and JBP923) and binding site residue (Glu595) of $PEPT_{so}$. The 7-hydroxy of JBP485 formed the hydrogen bond with the negative charge of Glu595. However, the amino of JBP923 and J3V could make ion-dipole interaction with Glu595. It is well known that the energies of hydrogen bond (2-8 kcal/mol) is smaller than that of ion−dipole interaction (>100 kcal/mol)[29], implying that J3V and JBP923 would presumably be more stably interacting with Glu595 of $PEPT_{so}$ as compared to JBP485. These results were consistent with our hypothesis that the pseudo-tripeptides would be accommodated by the binding pocket of PEPT1 and the N-terminal amino group of

amino acid introduced into the pseudo-tripeptide could interact highly with PEPT1.

Pharmacokinetic study

The PEPT1 seems to be highly conserved, in the aspect of sequence, tissue distribution, localization and function, between mammalian species. The PEPT1 gene sequences of rat (NM_057121.1) and beagle dog (NM_001003036) has >80% similarity to those of human (NM_005073)[30]. Similar intestinal distribution of PEPT1 and similar function in transporting its substrates in SD rats, beagle dogs and humans were observed as well[30-32]. So we performed the pharmacokinetic (PK) study to assess the absorptive rate, extent and mechanism of JBP485 and its prodrugs in rats and beagle dogs.

Pharmacokinetic profile of oral JBP485 and its prodrugs in rats

The oral bioavailability of prodrugs (J3V, J3I, J3L, J3P, J7V) compared to JBP485 was tested in SD rats following oral administration. Figure 7A summarized the plasma concentration-time profiles and Table 3 listed the pharmacokinetic parameters. The PEPT1 could allow for fast and efficient uptake of its substrates due to a high-capacity system, indicating small T_{max} and high AUC_{0-t} and C_{max} for the high affinity substrates. The T_{max} of J3V, J3I, J7V was 1.4-2.2-fold lower than that of JBP485. Also, the AUC_{0-t} and the C_{max} of J3V, J3I and J7V were approximately 1.5-2.4-fold and 1.5-4.1-fold greater than that of JBP485, respectively. J3V exhibited the highest bioavailability among these prodrugs, because L-valine might have the preferred combination of chain length and branch at the β-C of the amino acid, which facilitated the binding with PEPT1. However, J3P and J3L exhibited 2.4-2.8-fold decrease in oral bioavailability compared to JBP485 because of low affinity of PEPT1 and instability in the gastrointestinal tract.

To further evaluate the role of PEPT1 in the oral absorption of J3V in vivo, we conducted competitive inhibition study involving co-administration with Gly-Sar. The absolute bioavailability of J3V decreased from 50.1% to 27.1% in the presence of Gly-Sar and the inhibition ratio was 45.8% (Figure 8A, Table 4). The above results showed the competitive inhibition of Gly-Sar on the PEPT1-mediated transport of

J3V did occur in vivo, further indicating that the high bioavailability of J3V was made by enhanced affinity to PEPT1.

It had also been mentioned that JBP485 could interact with other influx transporters or regulate their expression, eg. PEPT2 (SLC *15A2*)[33], OCT2 (SLC *22A2*) and OAT1 (SLC *22A6*), OAT3 (SLC *22A8*)[34]. Considering the complex circumstances, it was very important to exclude the possibilities that the changes of PK parameters of JBP485 and J3V in rats were related to other transporters expect for PEPT1. The reasons were listed as followings: 1) OCT2[35, 36], PEPT2[9, 37], OATs (OAT1, OAT3)[35, 38], highly expressed in kidney but not in intestine, represented the renal reabsorption and secretory pathway for substrates in kidney. Additionally, Liu had reported that JBP485 alone could not up-regulate the expressions of OCT2, which could be irrespective of substrate induction[34]. Furthermore, valaciclovir was also substrates of PEPTs (PEPT1 and PEPT2) and OATs[39, 40], but the oral bioavailability of valaciclovir was significantly enhanced by targeting effectively the PEPT1 transporter in the apical side of enterocytes, not other transporters[41]. Consequently, we believed that the oral absorption of JBP485 and J3V through the intestinal wall was not related to its recognition as a substrate by OCT2, PEPT2 and OATs; 2) Although the expression of OATP-B, OCTs (OCT1 and OCT3) transporters is observed in intestine, the substrates are commonly characterized as the large hydrophobic anions for OATPs[35, 42] and the organic cations for OCTs[36]. Additionally, JBP485 and J3V were not the substrates proved by the inhibition kinetic assays (captopril for OATP-B and metformin for OCTs) in Figure 4C.

Even if PEPT1 is a high-capacity transporter, it is significant to determine whether PEPT1 shows capacity-limited absorption at high dose. The J3V and JBP485 were orally administered to the rats at doses of 12 and 100 mg/kg and the plasma concentrations of JBP485 were shown in Figure 8C-8D and Table 4. There was a proportional increase of C_{max} and AUC_{0-t} with dosing increase of J3V (Figure 8D), suggesting that PEPT1-mediated transport of J3V was not saturated at high dose in rats. However, the corresponding AUC_{0-t} and C_{max} of JBP485 did not increase

proportionally with dose over the 10-fold range after orally administration of JBP485 at the dose of 12 and 100 mg/kg, demonstrating that saturation of the plasma concentration occurred for oral administration of JBP485. Consequently, we can draw conclusions that the capacity absorption process at the high dose has been observed for the high-affinity substrates of PEPT1 and the pseudo-tripeptidization strategy could improve maximum transport capacity of PEPT1 for cyclic dipeptides.

Bioactivation sites study of J3V

A core issue in developing successful prodrugs is balancing the need for stability prior to absorption in the gastrointestinal tract and easily conversion to parent drug after absorption. To investigate the in vivo bioconversion sites of J3V, portal vein and systemic plasma concentrations of J3V and JBP485 were determined. According to the chemical stability study, we assumed that J3V could pass through the apical membrane of intestinal epithelia primarily in intact form. J3V was prone to be metabolized in the intestinal epithelium cells, with $AUC_{0\text{-}120min}$ value in the portal plasma for JBP485 and J3V of 119.2 nM*min/mL and 24.93 nM*min/mL, suggesting that the majority bioactivation of J3V did occur in the enterocytes. The underlying reason was that there were some hydrolytic enzymes contributing to bioconversion of J3V, agreeing well with the instability of J3V in the intestine homogenates. In the systemic circulation, only JBP485 could be detected in the systematic plasma, suggesting the liver was the second-role bioactivation site. (Figure 8B, Table 5).

Pharmacokinetic profile of oral JBP485 and J3V in Beagle dogs

To evaluate the pharmacokinetic study of JBP485 and J3V in beagle dogs, J3V and JBP485 were both orally administered to male beagle dogs. Figure 7B summarized the plasma concentration-time profiles and Table 3 listed the pharmacokinetic parameters. Compared to JBP485, J3V showed a 3.2-fold higher C_{max} (85.9 nM/mL for J3V versus 26.65 nM/mL for JBP485) and 2.6-fold higher AUC_{0-t} (233.25 nM*h/mL for J3V versus 89.15 nM*h/mL for JBP485) and 2.6-fold lower T_{max} (0.58 h for J3V versus 1.5 h for JBP485). J3V exhibited the higher bioavailability and shorter T_{max} in comparison with JBP485 after oral administration in beagle dogs, consistent with the pharmacokinetic study in rats. Moreover, no J3V

in the systematic plasma was observed, implying rapid enzymatic activation in the intestinal epithelium cells, liver and plasma.

Anti-hepatitis activities in vivo

Although J3V could increase oral bioavailability in comparison with JBP485, it is important to show that J3V also could maintain the pharmacological effect of JPB485 or even perform better. We investigated the protective effect of JBP485 and J3V on alpha-naphthylisothiocyanate (ANIT)-induced liver injury in SD rats, with ursodeoxycholate sodium (UDCA) as a positive control. To preferably observe the hepatoprotective effect of JBP485 and J3V, we selected three doses of JBP485 (6.25, 12.5 and 25 mg/kg) and four doses of J3V (3.125, 6.25, 12.5 and 25 mg/kg) for oral administration and two doses of JBP485 (6.25, 12.5 mg/kg) for intraperitoneal administration in accordance with the results of pharmacokinetics. As shown in Figure 9A, the serum total bilirubin (TBIL), an important indicator of cholestasis, was 13.0-fold higher in the ANIT-treated rats than in the control rats. The high level of serum TBIL in ANIT-treated rats was significantly reduced when rats were orally administered with UDCA (100 mg/kg), different dose of JBP485 and J3V and were intraperitoneally injected with different dose of JBP485. Additionally, JBP485 and J3V could decrease T-BIL in a dose-dependent manner. As expected, high-dose oral J3V (25 mg/kg) and intraperitoneal JBP485 (12.5 mg/kg) exhibited similar and excellent performance, which was also validated by similar oral absolute bioavailability in the pharmacokinetic study. Figure 9B-9C showed that the varying tendencies of serum alanine aminotransferase (ALT) and aspartate aminotransferase (AST), another biochemical indicator of hepatic cell damage, were similar to that of T-BIL.

To further evaluate the liver histological changes, the liver sections were stained by H&E. The mononuclear and polymorphonuclear of hepatocytes were shrunk and the cytoplasmic swelling was accompanied with massive necrosis in ANIT-treated rats by microscopic examination (Figure 10B). The arrows indicated that the ANIT-induced hepatocellular edema and necrosis were alleviated in rats after

treatment of UDCA, JBP485 and J3V, separately (Figure 10C-10L), which was consistent with the results of serology study. These results suggested that J3V could maintain remarkable hepatoprotective effects of JBP485 on ANIT-induced liver injury or even perform better.

CONCLUSIONS

In this study, we develop the bioactivatable pseudo-tripeptidization strategy of cyclic dipeptides to increase the binding affinity towards PEPT1, leading to enhanced intestinal permeability accompanied by better stability of prodrugs in the GI tract and enzymes-mediated bioactivation to the bioactive parent compound in the intestinal epitheliums and hepatic cells. Our findings disclosed that the bioactivatable pseudo-tripeptidization strategy of cyclic dipeptides could be adopted to improve oral absorption of cyclic dipeptides with no/low affinity toward PEPT1, which could provide more possibilities in clinical translation for cyclic dipeptides with high bioactivity.

EXPERIMENTAL SECTIONS

General Information

JBP923 (purity: 98.8%) were purchased from Zhejiang Ontores Biotech Co., Ltd. (Zhejiang, Hangzhou, China); L-Ser-L-Hyp-L-Gly was supplied from Zhejiang taihepna biotechnologies Co., Ltd; cyclo(L-Pro-Gly) (purity: 98.3%) were obtained from Anhui Research Peptide Biotechnology Co., Ltd. HBSS buffers and HEPES buffers were brought from Dalian Meilun Biotech Co., Ltd. (Liaoning, Dalian, China); The *ter*-butyloxycarbonyl (Boc) protected amino acids (Boc-L-Valine, Boc-L-Isoleucine, Boc-L-Phenylalanine, Boc-L-Leucine) were obtained from GL Biochem Co., Ltd (China, Shanghai); Carbodiimide (EDCI), 4-Dimethylamino-pyridine (DMAP), N-methylmorpholine (NMM), 1-hydroxybenzotriazole (HOBT), and dicyclohexylcarbodiimide (DCC) were purchased from Kaile Chemicals (Shanghai,China); Glycylsarcosine (Gly-Sar) was purchased from Sigma-aldrich (St. Louis, MO). All other chemicals used were

analytical grade available.

Synthesis of JBP485 and PEPT1-targeted prodrugs of JBP485

All compounds were analyzed by nuclear magnetic resonance(^{1}H NMR) and high resolution mass spectrometry (HRMS). The purity of JBP485 and PEPT1-targeted prodrugs was ≥ 95% as determined by high-performance liquid chromatography (HPLC).

Synthesis of JBP485

The synthesized procedure was shown in Figure 2A. The Cmpd1 (1g, 3.63 mol) was dissolved in 10 mL sodium acetate buffer (10 mM, pH 4.5) at 90 °C for 2 h. The mixture was purified on HPLC to obtain Cmpd2. The prepared mixture was frozen and lyophilized for 12 h to afford JPB485. The compound was obtained in 42% yield as a white solid: ^{1}H NMR (600 MHz, DMSO-d_6): δ 7.82 (s, 1H), 5.12 (d, J = 3.0 Hz, 1H), 4.70 (t, J= 5.8 Hz, 1H), 4.41-4.31 (m, 1H), 4.29 (d, J= 4.1 Hz, 1H), 4.07 (d, J = 4.8 Hz, 1H), 3.78-3.61 (m, 2H), 3.56 (dd, J =12.6, 4.7 Hz, 1H), 3.20 (d, J = 12.6 Hz, 1H), 2.05 (dd, J = 13.0, 6.3 Hz, 1H), 1.87 (ddd, J = 12.9, 11.3, 4.4 Hz, 1H); HRMS (ESI): [M +H], calculated 201.08698, found 201.08695.

Synthesis of JBP485-3-CH_2-O-Amino Acid (AA)

The synthesized procedure was shown in Figure 2B. A mixture of Cmpd3 (10 g, 24.4 mmol), Cmpd4 (3.48 ml, 29.33 mmol) and sodium carbonate (33.1 g, 29.3 mmol) was dissolved in DMF and stirred at room temperature (r.t.) for 12 h. The solvent was evaporated. The residues were dissolved in DCM and were washed by 5% H_3PO_4, H_2O, $NaHCO_3$, brine and dried over by Na_2SO_4 (anhydrous) and were filtered and concentrated under the vacuum to afford Cmpd5. The Cmpd5 (13.8 g, 24.4 mmol) was charged with 25% DEA/THF (140 ml) solution and cooled down to -5 ^{o}C with the protection of nitrogen. The solution was stirred under r.t. for 1 h. The reaction mixture was then concentrated under the vacuum and purified by column chromatography to afford Cmpd6. A mixture of Cmpd6, Cmpd7, EDCI, HOBt and NMM was fully dissolved in DCM and stirred for 2 h. The reaction mixture was then washed by 5% H_3PO_4, H_2O, $NaHCO_3$ (saturated solution), brine and dried over by

Na_2SO_4 (anhydrous). It was filtered and concentrated under the vacuum to afford oily product. It was purified by column chromatography (DCM/MeOH=1000/1 to 700/1) to afford Cmpd8. The Cmpd8 (6.2 g, 10.55 mmol) and 25% DEA/THF (50 mL) solution were mixed and stirred at -5 ^{o}C for 1 h. The reaction mixture was then concentrated under the high vacuum to afford Cmpd9. A mixture of Cmpd9 (660 mg, 1.1 mmol), Cmpd10a (245 mg, 1.1 mmol) or Cmpd10b (285 mg, 1.1 mmol) or Cmpd10c (256 mg, 1.1 mmol) or Cmpd10d (256 mg, 1.1 mmol), DCC and DMAP was fully dissolved in DCM and then cooled down to -5 ^{o}C with the protection of nitrogen. The reaction mixture was stirring under r.t. for 12 h. The reaction mixture was filtered and concentrated under the vacuum to afford Cmpd11a-11d. 8mL of the cleavage cocktail (TFA/Tis/H_2O=95/2.5/2.5) was cooled down to -5 ^{o}C and then Cmpd11a (800mg), Cmpd11b (928 mg), Cmpd11c (837 mg), Cmpd11d (837 mg) were added, respectively. The reaction mixture was stirred under r.t. for 1 h. The mixture was then precipitated into ether and was washed by ether thrice. The white precipitation formed was collected through centrifugation at 3500 rpm for 10 min and was purified on pre-HPLC to obtain Cmpd12a-12d. The Cmpd12a-12d were frozen and lyophilized for 12 h, respectively.

JBP485-3-CH_2-O-Val (J3V, 12a): The title compound was obtained in 25% yield as a white solid: ^{1}H NMR (600 MHz, DMSO-d_6): δ 8.40 (s, 3H), 8.27 (s, 1H), 4.55-4.47 (m, 2H), 4.43 (ddd, J = 11.5, 6.2, 1.6 Hz, 1H), 4.39 (dq, J = 8.8, 4.8 Hz, 1H), 4.32 (t, J = 4.5 Hz, 1H), 3.57 (dd, J = 12.6, 4.6 Hz, 1H), 3.24 (d, J = 12.6 Hz, 1H), 2.17 – 2.05 (m, 2H), 1.85 (ddd, J = 12.8, 11.4, 4.3 Hz, 1H), 0.95 (dd, J = 9.3, 7.0 Hz, 6H); HRMS (ESI): [M+H], calculated 300.15540, found 300.15510.

JBP485-3-CH_2-O-Phe (J3P, 12b): The title compound was obtained in 18% yield as a white solid: ^{1}H NMR (600 MHz, DMSO-d_6): δ 8.41 (s, 3H), 8.28 (s, 1H), 7.34 (dd, J = 8.0, 6.6 Hz, 2H), 7.31-7.22 (m, 3H), 4.54-4.41 (m, 3H), 4.40-4.26 (m, 3H), 3.53 (dd, J = 12.6, 4.6 Hz, 1H), 3.24 (d, J = 12.5 Hz, 1H), 3.14 (dd, J = 14.4, 6.3 Hz, 1H), 3.07 (dd, J = 14.4, 6.3 Hz, 1H), 2.08 (dd, J = 13.1, 6.3 Hz, 1H), 1.90 (ddd, J = 12.8, 11.2, 4.3 Hz, 1H); HRMS (ESI): [M+H], calculated 348.15540, found 348.15499.

JBP485-3-CH_2-O-Leu (J3L, 12c): The title compound was obtained in 15% yield as a white solid: ^{1}H NMR (600 MHz, DMSO-d_6): δ 8.31 (s, 2H), 8.27 (s, 1H), 5.21 (s, 1H), 4.49 (dt, J = 8.9, 3.3 Hz, 2H), 4.43 (ddd, J = 11.5, 6.2, 1.6 Hz, 1H), 4.36 (dd, J = 11.8, 5.8 Hz, 1H), 4.32 (t, J = 4.5 Hz, 1H), 3.95 (t, J = 7.2 Hz, 1H), 3.56 (dd, J = 12.6, 4.6 Hz, 1H), 3.25 (d, J = 12.6 Hz, 1H), 2.09 (dd, J = 13.0, 6.3 Hz, 1H), 1.85 (ddd, J = 12.7, 11.3, 4.3 Hz, 1H), 1.79-1.70 (m, J = 6.6 Hz, 1H), 1.64 (dt, J = 14.1, 7.2 Hz, 1H), 1.53 (dt, J = 14.2, 7.3 Hz, 1H), 0.86 (dd, J = 6.5, 5.3 Hz, 6H); HRMS (ESI): [M +H], calculated 314.17105, found 314.17094.

JBP485-3-CH_2-O-Ile (J3I, 12d): The title compound was obtained in 22% yield as a white solid: ^{1}H NMR (600 MHz, DMSO-d_6): δ 8.34 (s, 3H), 8.26 (s, 1H), 5.199 (s, 1H), 4.55-4.46 (m, 2H), 4.43 (ddd, J = 11.5, 6.2, 1.7 Hz, 1H), 4.39 (dd, J = 10.9, 3.9 Hz, 1H), 4.32 (s, 1H), 3.99 (d, J = 3.6 Hz, 1H), 3.56 (dd, J = 12.6, 4.7 Hz, 1H), 3.24 (d, J = 12.6 Hz, 1H), 2.09 (dd, J = 12.9, 6.2 Hz, 1H), 1.90-1.67 (m, 2H), 1.50-1.33 (m, 1H), 1.33-1.10 (m, 1H), 0.90 (d, J = 6.9 Hz, 3H), 0.83 (t, J = 7.4 Hz, 3H); HRMS (ESI): [M +H], calculated 314.17105, found 314.17098.

Synthesis of JBP485-7-O-Val (J7V, 19)

The synthesized procedure was shown in Figure 2C. A mixture of Cmpd13 (10 g, 26.1 mmol), Cmpd14 (4.71 g, 26.1 mmol), NMM, EDCI and HOBt was dissolved in DMF and stirred under r.t. for 2 h. The solvent was evaporated. The residues were dissolved in DCM and washed by 5% H_3PO_4, H_2O, $NaHCO_3$, brine and dried over by Na_2SO_4 (anhydrous). It was filtered and concentrated under the vacuum to afford oiley products. It was purified by column chromatography on a silica gel (DCM/MeOH=50/1 to 20/1) to afford Cmpd15. The Cmpd15 (6.8 g, 13.32 mmol) was charged with 25% DEA/THF solution and cooled down to -5 ^{o}C with the protection of nitrogen. The solution was stirred under r.t. to afford Cmpd16 and was concentrated under the vacuum. A mixture of Cmpd16 (2 g, 7.8 mmol), Cmpd17 (1.69 g, 7.8 mmol), DCC, DMAP was fully dissolved in DCM and stirred under r.t. for 12 h. The reaction mixture was filtered and concentrated under the vacuum to afford Cmpd18. 8 mL of cleavage cocktail (TFA/Tis/H_2O=95/2.5/2.5) was cooled down to -5°C and then Cmpd18 (800 mg) was added. The reaction mixture was stirred

under r.t. for 1 h. The mixture was then precipitated into ether and was washed by ether thrice. The white precipitation formed was collected through centrifugation at 3500 rpm for 10 min and was purified on pre-HPLC to obtain Cmpd19. The Cmpd19 was frozen and lyophilized for 12 h. The compound was obtained in 20% yield as a white solid: ^{1}H NMR (600 MHz, DMSO-d_6): δ 8.37 (s, 3H), 8.00 (s, 1H), 5.42 (t, J = 4.9 Hz, 1H), 4.78 (s, 1H), 4.41 (ddd, J = 11.5, 6.2, 1.7 Hz, 1H), 4.09 (td, J = 4.3, 1.6 Hz, 1H), 3.91 (d, J = 4.8 Hz, 1H), 3.87 (dd, J = 13.7, 5.1 Hz, 1H), 3.73 (d, J = 4.3 Hz, 2H), 3.43 (d, J = 13.7 Hz, 1H), 2.25 (dd, J = 13.8, 6.3 Hz, 1H), 2.22-2.13 (m, 2H), 0.99 (d, J = 7.0 Hz, 3H), 0.97 (d, J = 6.9 Hz, 3H); HRMS (ESI): [M +H], calculated 300.15540, found 300.15517.

Stability Study

Chemical stability

The chemical stability of JBP485 and its prodrugs was studied in buffers with various pHs (0.1 M HCl, pH 4.5 acetate buffer, pH 5.8 phosphate buffer, pH 6.8 phosphate buffer and pH 7.2 phosphate buffer) and simulated gastric fluids (SGF, pH 1.2) and simulated intestinal fluids (SIF, pH 6.8). Above solutions were prepared according to methods described in the Chinese Pharmacopoeia (2015 edition). JBP485 and its prodrugs were dissolved in buffers and simulated gastric/intestinal fluids to obtain the solutions with a concentration of 5 mM. 200 μL samples were taken at different time points (0, 0.25, 0.5, 1, 2, 4, 8, 12, 20 h) and analyzed by HPLC.

Metabolic stability

The metabolic stability study in rats was conducted in accordance with protocols approved by the Animal Care and Use Committee at Shenyang Pharmaceutical University. The jejunum and liver were excised from euthanized 6-week-old male Sprague-Dawley (SD) rats (weighing 200−250 g, no strains of animals) from Shenyang Pharmaceutical University and were washed with ice-cold PBS buffer at pH 7.4. The tissues which added to ice-cold PBS buffer at pH 7.4 were then homogenized by ultrasonic homogenizer and centrifuged at 3500 rpm for 10 min. The supernatant was collected and the protein content was obtained by the Bio-Rad DC

Protein Assay (Bio-Rad Laboratories Inc., Hercules, CA). The plasma was obtained from the rat jugular vein after centrifugation at 13000 rpm for 10 min. JBP485 and its prodrugs (5 mM) were incubated with liver (200 μg/mL of protein), intestinal homogenates (200 μg/mL of protein) and plasma at 37 °C. Samples (200mL) were taken at specific time points (0, 10, 20, 30, 60, 90, 120 min) and quenched with 600 μL of ice-cold acetonitrile, and then centrifuged at 13000 rpm (4 ℃) for 10 min. The supernatant was analyzed using HPLC.

Apparent first-order degradation kinetics and rate constants were measured by using rates of hydrolysis. The percentage of remaining pordrugs was plotted against corresponding time points, the half-life ($t_{1/2}$) obtained from linear regression of pseudo-first-order kinetics. The relation between the rate constants (k) and slopes of the plots is explained by the following equation:

$$k=2.303\times\text{slope (log C vs time)}$$

The $t_{1/2}$ is then calculated by the following equation:

$$t_{1/2} = \frac{0.693}{k}$$

Caco-2 membrane permeability

Caco-2 cells were seeded on 12-well transwell inserts (0.4 μm pore size, area 1.12 cm^2, Corning, NY) at a density of 1.0×10^4 cells/cm^2 and cultured in MEM (10% FBS, 1 mM sodium pyruvate, 1% non-essential amino acids and 1% L-glutamine; Invitrogen, Carlsbad, CA). Caco-2 Cells were cultured in 5% carbon dioxide and 90% humidity at 37 °C. Monolayers with transepithelial electrical resistance (TEER) values >300 Ω/cm^2 were used for the study. 0.5 mL of pH 6.0 Hank's balanced salt solution (HBSS) and 1.5 mL of pH 7.4 HBSS buffer were applied to the apical (AP) layer and the basolateral (BL) layer, respectively. The plates were maintained at 37 °C for 20 min. The AP layer medium was aspirated and replaced with 0.5mL of JBP485 and its prodrugs (0.5 mM) solution in pH 6.0 HBSS buffer and the BL layer medium was replaced with 1.5 mL of pH 7.4 HBSS buffers. 200 μL of samples from BL layer medium were collected at 5, 15, 30, 45 and 60 min for evaluating absorptive transport

and were replaced with HBSS buffers at pH 6.0. Each experiment was repeated three times. Drug concentrations were determined by the UPLC-MS/MS method and the apparent permeability coefficient (P_{app}) was calculated using the following formula.

$$P_{app} = \frac{dQ/dC}{AC}$$

where A is the surface area of the monolayer (cm^2), C is the initial concentration of JBP485 and its prodrugs (μmol) in the donor solution and dQ/dt is the steady-state flux (μmol/s).

Single-pass intestinal perfusion (SPIP) study in rats

According to the ethical guidelines for the care and use of laboratory animals of Shenyang Pharmaceutical University, animal experiments were conducted. The 6-week-old male Sprague-Dawley rats (SD rats, weighing 200−250 g, no strains of animals) were bought from Shenyang pharmaceutical University and were fasted for 12 h before the perfusion experiment. Briefly, SD rats were anesthetized with urethane (1.5 g/kg) by intraperitoneal injection and then fixed on an operation table at 37 °C. The abdomen was opened by a midline incision of 3-4 cm and about 10 cm of jejuna was carefully exposed. After the jejuna were cleared with saline solution (37 °C), one end was connected to a peristaltic pump (BT100, Changzhou Purui Precision Pump Co., Ltd., China) and the other end was connected to a collecting vial. The peristaltic pump rate was 0.2 mL/min. The HEPES buffer at pH 6.0 containing 5 mM of JBP485, JBP923 and J3V was used and the outflow samples were collected at 15, 30, 45, 60, 90, 120 min after the steady state at the rate of 0.2 mL/min. The length and radius of the jejuna were accurately measured at the end of the experiment. Samples (200 μL) were quenched with 600 μL of ice-cold acetonitrile and centrifuged at 13000 rpm (4 °C) for 10 min. The supernatant was analyzed using HPLC. The effective permeability (P_{eff}) was determined using the following equation:

$$P_{eff} = \frac{-Q\ln(C_{out}V_{out}/C_{in}V_{in})}{2\pi RL}$$

where Q is the perfusion buffer flow rate (0.2 mL/min) of the inlet solution, C_{out}/C_{in} is the ratio of the outlet and the inlet concentrations (μmol/mL) of tested compounds,

V_{out}/V_{in} is the ratio of the outlet and inlet volume (the density of perfusates is determined as 1 kg/L), R and L are the radius and length of the intestinal segment (cm), respectively.

Cellular Uptake Study

Caco-2 cells were seeded at a density of 1×10^4 cells/cm^2 in 24-well plates. The concentration- and proton-dependent transport of JBP485, J3V and JBP923 were made to validate the cellular uptake mechanism. The concentration-dependent uptake of JBP485, J3V and JBP923, ranging from 0.2 to 5 mM, was determined in Caco-2 cells with 10 min incubation at 37 ℃. The Michaelis-Menten constant (K_m) was calculated by Eadie–Hofstee plot. The Caco-2 cells were incubated with JBP485, J3V and JBP923 (0.5 mM) in the culture medium of either pH 6.0 or pH 7.4 HBSS buffer with 10 min for proton-dependent uptake. After incubation, cells were washed three times with ice-cold PBS at pH 7.4 to stop uptake. The cells were then homogenized in 0.3 mL water and 20 μL of suspension was used to determine protein content by the Bio-Rad DC Protein Assay. The remaining cell homogenization was centrifuged at 13000 rpm for 10 min, and then the supernatant of samples was collected stored at -80 °C until analysis by UPLC/MS/MS.

An inhibition assay was conducted using 0.5 mM Gly-Sar as a probe substrate to assess if the uptake of Gly-Sar was inhibited by JBP485, J3V and JBP923 (0.5 to 50 mM). The half-maximal inhibitory concentration (IC_{50}) values were obtained by Nonlinear data fitting (Graph Pad Prism V5.0). In addition, 50 mM Gly-Sar was assessed to determine their inhibitory on 0.5 mM JBP485, J3V and JBP923 uptake mediated by PEPT1. Furthermore, the inhibition study was also evaluated whether 50 mM captopril (the substrates for OATP-B) and metformin (the substrates for OCT1-3) could inhibit 0.5 mM JBP485 and J3V uptake.

Molecular docking

The amino acid sequence of human PEPT1 (hPEPT1) is solute carrier having 708 amino acids. According to the two-dimensional (2D) structure, ligands (JBP485,

J3V and JBP923) were built into three-dimensions using DS 3.0. We built homology models of PEPT1 based on prokaryotic $PEPT_{So}$ structures (PDB code: 4UVM, sequence identities of 35%) by automatic model of SWISS-MODEL server. All molecular docking experiments were performed with AutoDock Vina software. The other docking parameters were set to the default values. In order to improve the confidence level of the computer simulation, results with less than 2 Å root-mean-square deviations (RMSD) were accepted. The optimized parameters of simulations were as follows: as described previously[43]. Discovery Studio 4.0 Visualizer was used to display the interaction models between PEPT1 and ligands.

Pharmacokinetics study

Pharmacokinetic profile of oral JBP485 and its prodrugs in rats

All pharmacokinetic study in rats was conducted in accordance with protocols approved by the Animal Care and Use Committee at Shenyang Pharmaceutical University. The 5-week-old male SD rats (weighing 200−250 g, no strains of animals) were obtained from Shenyang Pharmaceutical University and were maintained on a 12 h light−dark cycle with access to food and water. The rats were fasted but had free access to water for 12 h before experiments. Six groups of SD rats (n=6, technical replicates) were orally treated with JBP485, J3V, J3I, J3L, J3P and J7V at a JBP485 dose of 12 mg/kg. To calculate the absolute bioavailability, JBP485 was also given intravenously to rats at a dose of 6 mg/kg. J3V (12 mg/kg, calculate as JBP485) was administrated to rats alone or with Gly-Sar (100 mg/kg) to verify whether J3V was the substrate of PEPT1 or not. In addition, J3V (12 and 100 mg/kg, calculated as JBP485) and JBP485 (12 and 100 mg/kg) were orally administered to rats to investigate the dose effects. Blood samples (200 μL) were withdrawn from the jugular vein at 0.083, 0.167, 0.333, 0.5, 1, 2, 4, 6, 8, 10 h and then centrifuged (13000 rpm, 4 °C for 10 min), respectively. The supernatant of samples was stored at -80 °C until UPLC-MS/MS analysis. The absolute bioavailability of JBP485 and its prodrugs was calculated using the following equation.

$$F = \frac{AUC_{po} \times D_{iv}}{AUC_{iv} \times D_{po}} \times 100\%$$

where F is the absolute oral bioavailability, AUC_{po} and AUC_{iv} are the area from time zero to the last time point under the plasma concentration-time curves of oral and intravenous administration, respectively. D_{po} and D_{iv} are the oral and intravenous administration doses, respectively.

Bioactivation sites study of J3V

The systemic and hepatic portal pharmacokinetics of J3V was evaluated to investigate the bioactivation sites in rats after an oral administration of J3V (12 mg/kg, calculated as JBP485). Portal vein and jugular samples were withdrawn simultaneously at 15, 30, 60, 120 min and then centrifuged (13000 rpm, 4 °C for 10 min), respectively. The supernatant of samples was stored at -80 °C until bioanalysis.

Pharmacokinetic study in Beagle dogs

The pharmacokinetic study in beagle was conducted in accordance with the guidelines recommended by the Animal Care and Use Committee at Shenyang Pharmaceutical University. The 2-year-old male beagle dogs (weighing 8-10 kg, no strains of animals) obtained from Shenyang Pharmaceutical University were orally administered with JBP485 (12 mg/kg) and J3V (12 mg/kg, calculated as JBP485) in aqueous solution. Blood samples (1 mL) were collected from the jugular vein via direct vein puncture at 0.167, 0.25, 0.33, 0.5, 1, 2, 4, 6, 8 h and placed into sodium heparin tubes. Blood samples were centrifuged at 13000 rpm for 10 min at 4 °C and collected in tubes and stored at -80 °C until bioanalysis.

Anti-hepatitis activities in vivo

The 6-weeks-old male SD rats (weighing 200-250 g, no strains of animals) were purchased from Shenyang Pharmaceutical University. All pharmacokinetic study in rats was conducted in accordance with protocols approved by the Animal Care and Use Committee at Shenyang Pharmaceutical University. The rats were fasted but had free access to water for 12 h before experiments. 1-Naphthyl isothiocyanate (ANIT)

was dissolved in olive oil and compounds (JBP485 and J3V) were dissolved in water and ursodeoxycholate sodium (UDCA) was suspended in 5% sodium carboxymethylcellulose (CMC-Na) solution. The animals were randomly divided into 12 groups with 6 rats in each group as following: Group 1: The rats served as normal control and received water at 30 min before and 8, 22, 32 and 46 h after olive oil was intraperitoneally (i.p) injected; Group 2: the rats were i.p injected at the dose of 50 mg/kg ANIT to induce cholestasis; Group 3: UDCA was orally administered to the ANIT-treated rats at doses of 100 mg/kg at 30 min before and 8, 22, 32 and 46 h after ANIT treatment; Group 4-6: JBP485 was orally administered to the ANIT-treated rats at doses of 6.25, 12.5 and 25 mg/kg in the same manner as described in Group 3; Group 7-8: JBP485 was i.p injected to the ANIT-treated rats at doses of 6.25, 12.5 mg/kg in the same manner as described in Group 3; Group 9-12: J3V was orally administered to the ANIT-treated rats at doses of 3.125, 6.25, 12.5 and 25 mg/kg in the same manner as described in Group 3. Serum was collected 48 h after ANIT treatment for determining hepatic biochemical index. For serum collection, rats were anesthetized with chloral hydrate and blood was collected from abdominal aorta. Blood was then left on the coagulation-promoting tubes and centrifuged for 5 min at 3500 rpm to obtain the supernatant as serum. The total bilirubin concentration (T-BIL) and the activity of liver specific cytosolic enzymes (ALT and AST) in the rat serum were determined using the appropriate assay kits (Nanjing Jiancheng Pure Chemical Industries). Moreover, the cut liver was immersed in 4% triformol solutions and stained with hematoxylin–eosin (H&E) for morphological examination.

Analytical methods

Pre-HPLC Analysis JBP485 and its prodrugs were purified by preparative high performance liquid chromatography (pre-HPLC) (Hitachi Technologies, Japan) that consist of a Hitachi L-2130 pump, Hitachi L-2420 UV detector. Separation was achieved using a C_{18} column (250 mm×20 mm, 5 μm) maintained at 30 °C with a mobile phase consisting of methol:water (5:95, v/v) for JBP485 and methol:water:hydrochloric acid (5:95:0.1, v/v/v) for all prodrugs.

HPLC Analysis The samples from purity study of JBP485 and its prodrugs were analyzed by Hitachi HPLC instrument (Hitachi Technologies, Japan) that consist of a Hitachi 1110 pump, Hitachi 1210 auto sampler, and Hitachi 1410 UV detector. Separation was achieved using a C_{18} column (25mm×4.6mm, 5μm) maintained at 30 °C with a mobile phase consisting of methol:water (5:95, v/v) for JBP485 and acetonitrile:water:trifluoroacetic acid (5:95:0.1, v/v/v) for all prodrugs. The flow rate was 1.0 mL/min and the UV detection were carried out at 205 nm.

The samples from stability study and SPIP study of JBP485 and its prodrugs were analyzed by WATERS e2695 HPLC instrument (WATERS Technologies, CA, USA) that consist of a WATERS e2695 pump, WATERS e2695 autosampler, and WATERS 2489 UV detector. Separation was achieved using a C_{18} column (25mm×4.6mm, 5μm) maintained at 30 °C with a mobile phase consisting of acetonitrile:water:trifluoroacetic acid (5:95:0.1, v/v/v). The flow rate was 1.0 mL/min and the UV detection were carried out at 205 nm.

UPLC-MS-MS Analysis Cell samples from monolayer permeability study and cellular uptake study and plasma samples from pharmacokinetic study were analyzed using ultra performance liquid chromatography–dual mass spectrometry (UPLC–MS/MS) method performed on ACQUITY UPLC^{TM} system (Waters Corp., Milford, MA). Prior to analysis, frozen samples were thawed on ice. The samples (50 μL) were processed using a protein precipitation method by addition of 50 μL of internal standard (cyclic (L-Pro-L-Gly), 0.1 μM) dissolved in acetonitrile and 100 μL of acetonitrile, followed by vortex mixing for 30 s and then centrifugation at 13000 rpm for 10 min at 4 °C. A 150 μL aliquot of supernatant was dried by nitrogen and the dried samples were reconstituted by solutions containing 50 μL of acetonitrile and 50 μL of water. A volume of 10 μL was injected into the liquid chromatography instrument for quantitative analysis. The separations were carried out on the C_{18} column (50 mm×2.1 mm, 1.7 μm; Waters Corp.) with mobile phase composed of methanol/water/acetic acid (5/95/0.1, v/v/v). In the MS/MS detector, the cone voltage was maintained at 35 V, collision energy was at 18 eV and argon collision gas pressure was 4.0×10^{-3} mbar. Data acquisition was by multiple reactions monitoring in

positive ion electrospray ionization mass spectrometry. The compounds were analyzed by multiple reaction monitoring of the transitions of m/z 200.1→86.2 for JBP485, m/z 300.3→72.1 for J3V, m/z 314.3→72.1 for J3I, m/z 314.3→72.1 for J3L, m/z 348.3→72.1 for J3P, m/z 300.3→72.1 for J7V, m/z 219.2→86.0 for JBP923, and 155.2→70.0 for internal standard, respectively.

Statistical analysis

All the quantitative data were expressed as their mean±S.D. (standard deviation), and the statistical analysis was made using the ANOVA test. The differences were considered to be statistically significant at $p < 0.05$

SUPPLEMENT INFORMATION

Additional supporting documents are available, including 1H NMR, HRMS spectra and HPLC chromatography of JBP485 and its prodrugs (J3V, J3L, J3P, J3I, J7V) and the 3D pdb files for docking of JBP485, JBP923 and J3V inside the binding site of hPEPT1

.

AUTHOR INFORMATION

Corresponding Authors

* Zhonggui He. E-mail address: hezhonggui@vip.163.com.

* Jin Sun. E-mail address: sunjin66@21cn.com.

ORCID

Zhonggui He: 0000-0002-5907-3875

Jin Sun: 0000-0001-7385-9017

Notes

The authors declare no competing financial interest.

ACKNOWLEDGEMENT

This work was financially supported by the National Nature Science Foundation of China (No. 81773656, 81573497, U1608283) and Key Projects of Technology Bureau in Shenyang (No18400408) and the Key Projects of Liaoning Province

Department of Education (No. 2017LZD03).

ABBREVIATIONS USED

PEPT1, oligopeptide transporter 1; JBP485, cyclo(L-Hyp-L-Ser); JBP923, L-Hyp-L-Ser; J3V, JBP485-3-CH_2-O-Valine; J3L, JBP485-3-CH_2-O-Leucine; J3I, JBP485-3-CH_2-O-Isoleucine; J3P, JBP485-3-CH_2-O-Phenylalanine; J7V, JBP485-7-O-Valine; Boc-, *ter*-butyloxycarbonyl-; EDCI, Carbodiimide; DMAP, 4-Dimethylamino-pyridine; NMM, N-methylmorpholine; HOBT, 1-hydroxybenzotriazole; DMF, dimethylformamide; DCM, dichloromethane; DCC, dicyclohexylcarbodiimide; r.t., room temperature; Gly-Sar: glycylsarcosine; DPK, diketopiperazine; GI, gastrointestinal; K_i, inhibition constant; HPLC, high-performance liquid chromatography; NMR, nuclear magnetic resonance; MS: mass spectrometry; UPLC-MS/MS, ultra performance liquid chromatography-dual mass spectrometry; $t_{1/2}$, half-time; FBS, fetal bovine serum; IC_{50}, half-maximal inhibitory concentration; TEER, transepithelial electrical resistance; P_{app}, apparent permeability coefficient; HBSS, Hank's balanced salt solution; AP: apical; BL: basolateral; SPIP: single-pass intestinal perfusion; K_m, michaelis constant; i.v., intravenous; 2D structure, two-dimensional structure; SD rats: Sprague-Dawley rats; PDB, Protein Data Bank; S.D., standard deviation.

REFERENCES

1. Bellezza, I.; Peirce, M. J.; Minelli, A. Cyclic dipeptides: from bugs to brain. Trends Mol. Med. 2014, 20, 551-558.

2. Kwak, M.-K.; Liu, R.; Kang, S.-O. Antimicrobial activity of cyclic dipeptides produced by lactobacillus plantarum LBP-K10 against multidrug resistant bacteria, pathogenic fungi, and influenza A virus. Food Control 2018, 85, 223-234.

3. Song, M. K.; Rosenthal, M. J.; Hong, S.; Harris, D. M.; Hwang, I.; Yip, I.; Golub, M. S.; Ament, M. E.; Go, V. L. W. Synergistic antidiabetic activities of zinc, cyclo (His-Pro), and arachidonic acid. Metabolism 2001, 50, 53-59.

4. David, T.; Thwaites, B.; H. H.; Nicholas L. Simmons. Passive transepithelial absorption of thyrotropin-releasing hormone (TRH) via a paracellular route in cultured intestinal and renal

epithelial cell lines. Pharm. Res. 1993, 10, 674-681.

5. Liu, Z.; Wang, C.; Liu, Q.; Meng, Q.; Cang, J.; Mei, L.; Kaku, T.; Liu, K. Uptake, transport and regulation of JBP485 by PEPT1 in vitro and in vivo. Peptides 2011, 32, 747-754.

6. Balvinder S. Vig.; T. R. S.; Julita K.; Timoszy K.; Quan Y.; Teresa N. Faria. Human PEPT1 pharmacophore distinguishes between dipeptide transport and binding. J. Med. Chem. 2006, 49, 3636-3644.

7. Mizuma, T.; T. N.; A. S.; Concentration-dependent a typical intestinal absorption of cyclic phenylalanyserine: small intestine acts as an interface between the body and ingested compounds. Biol. Pharm. Bull. 2003, 26, 1625-1628.

8. Tamura, K.; Philip, L.; Smith, Ronald T.; Borchardt. Effect of charge on oligopeptide transporter-mediated permeability of cyclic dipeptides across Caco-2 cell monolayers. Pharm. Res. 1996, 13, 1752-1754.

9. Terada, T.; Sawada, K.; Irie, M.; Saito, H.; Hashimoto, Y.; Inui, Ki. Structural requirements for determining the substrate affinity of peptide transporters PEPT1 and PEPT2. Pflug. Arch. Eur. J. Phy. 2000, 440, 679-684.

10. Giovanni M. Pauletti.; S. G.; Teruna J.; Siahaan, Jeffrey Aube.; Ronald T. Borchardt. Improvement of oral peptide bioavailaiblity: peptidomimeitcs and prodrug strategies. Adv. Drug Deliver. Rev. 1997, 27, 235-256.

11. Li L.; C. W.; Liu K. Preparation, in vitro release and pharmacokinetics of JBP485-loaded PLGA nanoparticles for oral delivery. Central South Pharmacy 2016, 14, 932-935.

12. Lei Li, C. W., Liu K. Preparation and pharmacokinetics of JBP485-loaded W/O microemulsion for oral delivery. Herald Med. 2014, 2, 135-139.

13. Liu, D.; Zhang, H.; Fontana, F.; Hirvonen, J. T.; Santos, H. A. Current developments and applications of microfluidic technology toward clinical translation of nanomedicines. Adv. Drug Deliv. Rev. 2018, 128, 54-83.

14. Luo, C.; Sun, J.; Sun, B.; He, Z. Prodrug-based nanoparticulate drug delivery strategies for cancer therapy. Trends Pharmacol. Sci. 2014, 35, 556-566.

15. Marquez, R.; Forgiarini, A. M.; Langevin, D.; Salager, J. L. Instability of emulsions made with surfactant-oil-water systems at optimum formulation with ultralow interfacial tension. Langmuir 2018, 34, 9252-9263.

16. Sun, J.; Dahan, A.; Amidon, G. L. Enhancing the intestinal absorption of molecules containing the polar guanidino functionality: a double-targeted prodrug approach. J. Med. Chem. 2010, 53, 624-632.

17. Murakami, T. A Minireview: Usefulness of transporter-targeted prodrugs in enhancing membrane permeability. J. Pharm. Sci. 2016, 105, 2515-2526.

18. Vig, B. S.; Huttunen, K. M.; Laine, K.; Rautio, J. Amino acids as promoieties in prodrug design and development. Adv. Drug Delivr. Rev. 2013, 65, 1370-1385.

19. Mitsuru Sugawara, W. H.; Fei, Y.; Malliga E.; Ganapathy. Transport of valganciclovir, a ganciclovir prodrug, via peptide transporters PEPT1 and PEPT2. J. Pharm. Sci. 1999, 89, 781-789.

20. Yan, Z.; Sun, J.; Chang, Y.; Liu, Y.; Fu, Q.; Xu, Y.; Sun, Y.; Pu, X.; Zhang, Y.; Jing, Y.; Yin, S.; Zhu, M.; Wang, Y.; He, Z. Bifunctional peptidomimetic prodrugs of didanosine for improved intestinal permeability and enhanced acidic stability: synthesis, transepithelial transport, chemical stability and pharmacokinetics. Mol. Pharm. 2011, 8, 319-329.

21. Zhang, Y.; Sun, J.; Gao, Y.; Jin, L.; Xu, Y.; Lian, H.; Sun, Y.; Sun, Y.; Liu, J.; Fan, R.; Zhang, T.; He, Z. A carrier-mediated prodrug approach to improve the oral absorption of antileukemic drug decitabine. Mol. Pharm. 2013, 10, 3195-3202.

22. Sun, Y.; Sun, J.; Shi, S.; Jing, Y.; Li, G.; Xu, Y.; He, Z. Synthesis, transport and pharmacokinetics of 5′-amino acid ester prodrugs of D-arabinofuranosylcytosine. Mol. Pharm. 2009, 6, 315-325.

23. Yagi A, N.; Okamura N.; Ishizu T.; Itoh H.; Shida T. Effect of cyclo(trans-4-L-hydroxyprolyl-L-serine) from hydrolysate of human placenta on baby hamster kidney-21/C-13 cells. Nat. Med. 1998, 52, 156-159.

24. Liu K.; O. L.; Kaku T.; Effect of Laennec on liver regeneration. Clin. Pharmacol. Ther. 1995, 5, 2187-2194.

25. Liu, K.; Y. K.; Kaku, T.; Santa, T. Kazuhiro, I.; Yagi, A.; Ishizu, T.; Sugiyama, Y. Hydroxyprolylserine derivatives JBP923 and JBP485 exhibit the antihepatitis activities after gastrointestinal absorption in rats. J. Pharmacol. Exp. Ther. 2000, 294, 510-515.

26. Cang, J.; Wang, C.; Liu, Q.; Meng, Q.; Wang, D.; Sugiyama, Y.; Tsuji, A.; Kaku, T.; Liu, K. Pharmacokinetics and mechanism of intestinal absorption of JBP485 in rats. Drug Metab. Pharmacok. 2010, 25, 500-507.

27. Colas, C.; Masuda, M.; Sugio, K.; Miyauchi, S.; Hu, Y.; Smith, D. E.; Schlessinger, A. Chemical modulation of the human oligopeptide transporter 1, hPepT1. Mol. Pharm. 2017, 14, 4685-4693.

28. Fowler, P. W.; Orwick-Rydmark, M.; Radestock, S.; Solcan, N.; Dijkman, P. M.; Lyons, J. A.; Kwok, J.; Caffrey, M.; Watts, A.; Forrest, L. R.; Newstead, S. Gating topology of the proton-coupled oligopeptide symporters. Structure 2015, 23, 290-301.

29. Sinko, P. J. State of Substance. Martin's physical pharmacy and pharmaceutical sciences, 6th ed 2009, 19-20.

30. Perkins, E. J.; Abraham, T. Pharmacokinetics, metabolism, and excretion of the intestinal peptide transporter 1 (SLC15A1)-targeted prodrug (1S,2S,5R,6S)-2-[(2'S)-(2-amino)propionyl]aminobicyclo[3.1.0.]hexen-2,6-dicarboxylic acid (LY544344) in rats and dogs: assessment of first-pass bioactivation and dose linearity. Drug metab. Dispos. 2007, 35, 1903-1909.

31. Englund, G.; Rorsman, F.; Ronnblom, A.; Karlbom, U.; Lazorova, L.; Grasjo, J.; Kindmark, A.; Artursson, P. Regional levels of drug transporters along the human intestinal tract: co-expression of ABC and SLC transporters and comparison with Caco-2 cells. Eur. J. Pharm. Sci. 2006, 29, 269-277.

32. Lu, H.; Klaassen, C. Tissue distribution and thyroid hormone regulation of PEPT1 and PEPT2 mRNA in rodents. Peptides 2006, 27, 850-857.

33. Guo, X.; Meng, Q.; Liu, Q.; Wang, C.; Sun, H.; Kaku, T.; Liu, K. Construction, identification and application of HeLa cells stably transfected with human PEPT1 and PEPT2. Peptides 2012, 34, 395-403.

34. Wen, S.; Wang, C.; Liu, K. JBP485 attenuates vancomycin-induced nephrotoxicity by regulating the expressions of organic anion transporter (Oat) 1, Oat3, organic cation transporter 2 (Oct2), multidrug resistance-associated protein 2 (Mrp2) and P-glycoprotein (P-gp) in rats. Toxicol. Lett. 2018, 295, 195-204.

35. Zhou, F.; Zhu, L.; Wang, K.; Murray, M. Recent advance in the pharmacogenomics of human solute carrier transporters (SLCs) in drug disposition. Adv. Drug Deliv. Rev. 2017, 116, 21-36.

36. Motohashi, H.; Y, S.; Inui, K. Gene expression levels and immunolocalization of organic ion

transporters in the human kidney. J. Am. Soc. Nephrol. 2002, 13, 866-874.

37. Ken-ichi, T.; T., Satohiro Masuda.; Hideyuki Saito. Physiological and pharmacological implications of peptide transporters, PEPT1 and PEPT2. Nephrol. Dial. Transpl. 2000, 15, 11-13.

38. George, B.; You, D.; Joy, M. S.; Aleksunes, L. M. Xenobiotic transporters and kidney injury. Adv. Drug Deliv. Rev. 2017, 116, 73-91.

39. Yue Z.; J. S.; Li H.; Li H. Association between concomitant use of acyclovir or valacyclovir with NSAIDs and an increased risk of acute kidney injury: data mining of FDA adverse event reporting system. Biol. Pharm. Bull. 2018, 41, 158-162.

40. Takeda M.; S. K.; Narikawa S.; Endou H. Human organic anion transporters and human organic cation transporters mediate renal antiviral transport. J. Pharmacol. Exp. Ther. 2002, 300, 918-924.

41. Yang, B.; Hu, Y.; Smith, D. E. Impact of peptide transporter 1 on the intestinal absorption and pharmacokinetics of valacyclovir after oral dose escalation in wild-type and PepT1 knockout mice. Drug metab. Dispos. 2013, 41, 1867-1874.

42. Kazuhiko Kato, Y. S.; Kuraoka, E.; Kikuchi, A.; Iguchi, M.; Suzuki, H.; Shibasaki, S.; Kurosawa, T.; Tamai, I. Intestinal absorption mechanism of tebipenem pivoxil, a novel oral carbapenem: involvement of human OATP family in apical membrane transport. Mol. Pharm. 2010, 7, 1747-1756.

43. Luo, Q.; Gong, P.; Sun, M.; Kou, L.; Ganapathy, V.; Jing, Y.; He, Z.; Sun, J. Transporter occluded-state conformation-induced endocytosis: amino acid transporter ATB (0,+)-mediated tumor targeting of liposomes for docetaxel delivery for hepatocarcinoma therapy. J. Control. Release 2016, 243, 370-380.

TABLE

Table 1. Stability of JBP485 and its prodrugs in different pH buffers, simulated gastric/intestinal fluids, rat intestinal/liver homogenates and plasma at 37 °C

Media	$T_{1/2}$ (h)					
	JBP485	J7V	J3I	J3V	J3L	J3P
0.1M HCL	>20	>20	>20	>20	>20	>20
pH 4.5 acetate buffer	>20	>20	>20	>20	>20	>20
pH 5.8 phosphate buffer	>20	>20	>20	>20	14.7	8.2
pH 6.8 phosphate buffer	>20	11.4	11.6	7.7	2.6	2.6
pH 7.4 phosphate buffer	>20	11.6	9.6	5.5	1.9	2.3
simulated gastric fluids	>20	>20	>20	>20	>20	>20
simulated intestinal fluids	>20	11.1	10.9	7.9	2.4	2.8
Intestine homogenates	>20	0.9	0.8	<0.16	<0.083	<0.083
Liver homogenates	>20	2.1	4.8	0.86	0.16	0.16
plasma	>20	6.1	4.0	2.9	0.32	0.29

Table 2. The concentration-dependent uptake of JBP485, J3V and JBP923 in Caco-2 cells. The Michaelis-Menten constant (K_m) was calculated by Eadie–Hofstee plot; the Gly-Sar competitive inhibition by JBP485, J3V and JBP923 in the Caco-2 cells, the uptake inhibition in Caco-2 Cells was denoted by IC_{50} values in mM. Data presented as mean ± SD; n=3, technical replicates. *P < 0.05 vs control and **P <0.01 vs control. The inset P values indicate the significance between groups.

	K_m (mM)	IC_{50} (mM)
JBP485	2.53±0.32	18.20±5.13
J3V	0.86±0.19*	2.90±0.98**
JBP923	0.65±0.26*	1.76±0.35**

Table 3. Pharmacokinetic parameters of JBP485 released from JBP485 and its prodrugs, following the oral administration of JBP485, J3V, J7V, J3I, J3P, and J3L to male SD rats (n=6, technical replicates) at a JBP485 dose of 12 mg/kg and intravenous administration of JBP485 at 6 mg/kg in rats and following the oral administration of JBP485 and J3V to male beagle dogs (n=6, technical replicates) at a JBP485 dose of 12 mg/kg[a]. *P < 0.05 vs control. The inset P values indicate the significance between groups.

	AUC_{0-t} (nM/mL*h)	C_{max} (nM/mL)	T_{max} (h)	$T_{1/2}$ (h)	F (%)
		Rats			
JBP485 (i.v)	194.0±31.53	334.91±85.135	-	1.13±0.16	-
JBP485 (p.o)	81.4±46.63	27.84±4.61	1.25±0.5	2.12±0.65	21.0
J3V (p.o)	194.47±23.87*	113.38±22.69*	0.57±0.25*	2.11±0.95	50.1*
J7V (p.o)	139.78±27.35*	98.26±17.22*	0.41±0.17*	2.51±0.99	36.0*
J3I (p.o)	122.65±26.9	41.80±19.50*	0.90±0.22*	0.90±0.22*	31.6*
J3P (p.o)	33.9±8.85	10.70±2.85*	1.00±0.61	2.38±1.41*	8.7*
J3L (p.o)	28.75±10.35	8.95±3.30*	1.30±0.67	2.23±0.79*	7.4*
		Beagle dogs			
JBP485 (p.o)	89.15±41.95	26.65±10.1	1.50±0.54	5.23±5.95	-
J3V (p.o)	233.25±58.15*	85.9±16.35*	0.58±0.20*	1.68±0.45	-

[a] Legend: AUC_{0-t}, area under the plasma concentration-time profiles from time zero to the last time point; $T_{1/2}$, elimination half-life; C_{max}, peak plasma concentration; T_{max}, time to reach the peak plasma concentration; F, absolute bioavailability.

Table 4. Pharmacokinetic parameters of JBP485, following oral administration of J3V to male SD rats (n=6, technical replicates) at 12 mg/kg with or without the presence of Gly-Sar 50 mg/kg, 100 mg/kg and oral administration of JBP485 to SD rats (n=6, technical replicates) at 12 mg/kg and 100 mg/kg[a]. *P < 0.05 vs control. The inset P values indicate the significance between groups.

Compound	J3V	
Dose	12mg/kg	12mg/kg+Gly-Sar
$T_{1/2}$ (h)	1.11±0.28	1.69±0.5
T_{max} (h)	0.58±0.29	0.5±0
C_{max} (nM/mL)	101.15±22.4	51.35±11.0*
AUC_{0-t} (nM/mL*h)	185.85±25.55	100.55±16.8*
Inhibition ratio	100%	45.8%
Compound	J3V	
Dose	12 mg/kg	100 mg/kg
$T_{1/2}$ (h)	1.29±0.27	1.28±0.14
T_{max} (h)	0.87±0.25	0.63±0.25
C_{max} (nM/mL)	113.49±19.76	1236.0±230.20
AUC_{0-t} (nM/mL*h)	249.78±24.63	2519.5±247.20
Compound	JBP485	
Dose	12 mg/kg	100 mg/kg
$T_{1/2}$ (h)	2.12±0.65	1.5±0.42
T_{max} (h)	1.25±0.50	1.5±1.43
C_{max} (nM/mL)	27.84±4.61	95.96±23.91
AUC_{0-t} (nM/mL*h)	81.4±46.63	323.55±78.30

[a] Legend: AUC_{0-t}, area under the plasma concentration-time profiles from time zero to the last time point; $T_{1/2}$, elimination half-life; C_{max}, peak plasma concentration; T_{max}, time to reach the peak plasma concentration.

Table 5. Pharmacokinetic parameters of J3V and JBP485 released from J3V in the hepatic portal and systemic circulation, following oral administration of J3V to male SD rats (n=4, technical replicates) after a 12 mg/kg (calculated as JBP485) [a].

	Portal		System	
	JBP485	J3V	JBP485	J3V
$AUC_{0\text{-}t}$ (nM/mL*min)	119.20±6.70	24.93±5.08	137.59±22.12	-
C_{max} (nM/mL)	93.15±6.60	22.21±3.89	114.63±24.63	-
T_{max} (min)	30	30	30	-

[a] Legend: $AUC_{0\text{-}t}$, area under the plasma concentration-time profiles from time zero to the last time point; $T_{1/2}$, elimination half-life; C_{max}, peak plasma concentration; T_{max}, time to reach the peak plasma concentration.

FIGURE

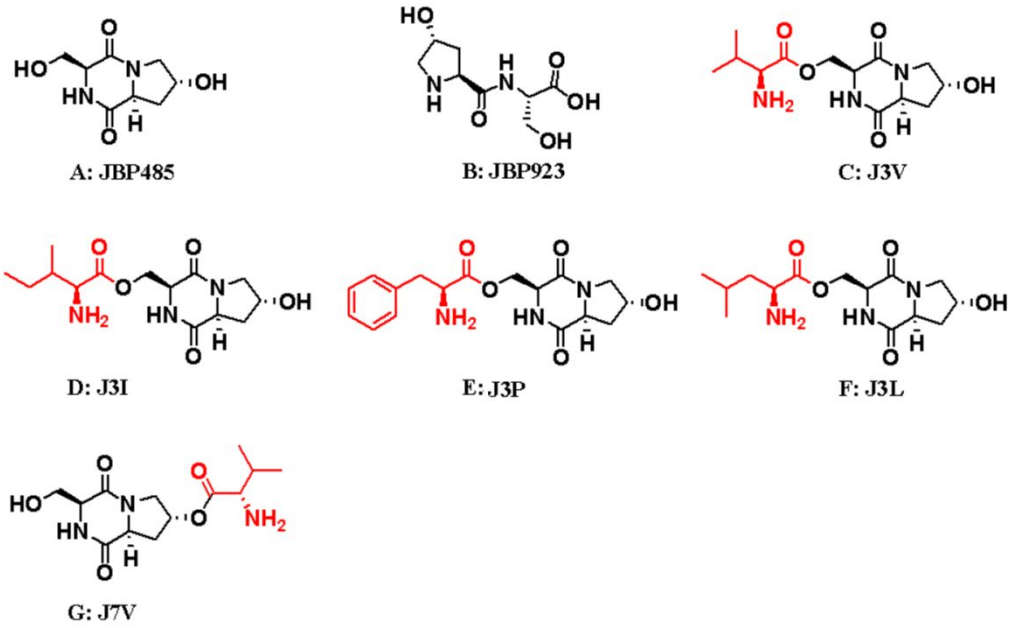

Figure 1. Chemical structures of JBP923, JBP485 and its prodrugs: (A) JBP485, (B) JBP923, (C) JBP485-3-CH_2-O-L-Valine (J3V), (D) JBP485-3-CH_2-O-L-Isoleucine (J3I), (E) JBP485-3-CH_2-O-L-Phenylalanine (J3P), (F) JBP485-3-CH_2-O-L-Leucine (J3L), (G) JBP485-7-O-L-Valine (J7V).

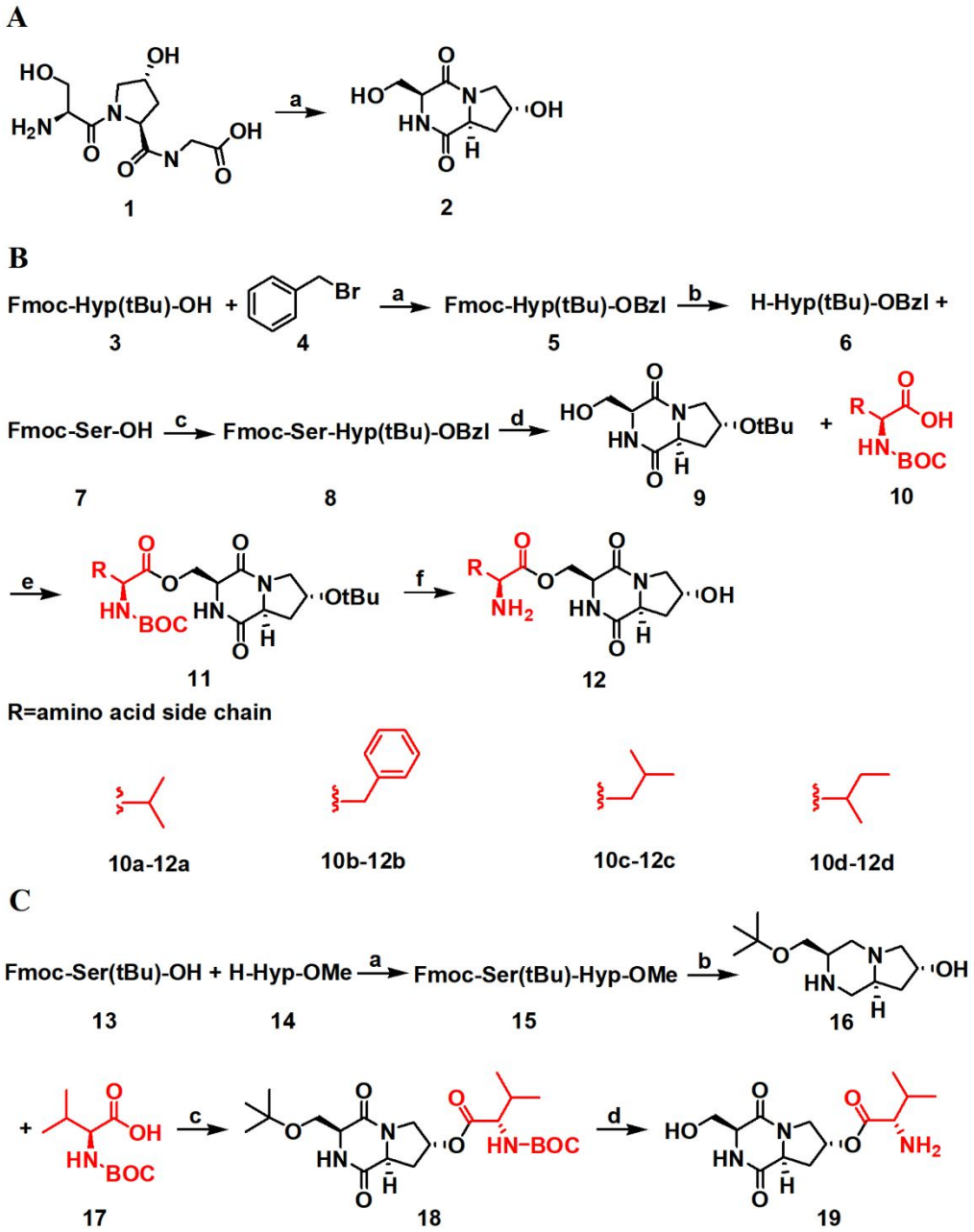

Figure 2. Synthetic routes for preparing JBP485 and its prodrugs: (A) Synthetic route to JBP485: (a) pH4.5 acetate buffer, 90 ℃, 2 h; (B) Synthetic route to JBP485-3-CH_2-O-AA: (a) sodium carbonate (Na_2CO_3), DMF; (b) diethylamine (DEA), THF; (c) EDCI, HOBT; (d) DEA, THF; (e) DCC, DMAP; (f) Tis, TFA, H_2O; (C) Synthetic route to J7V: (a): EDCI，HOBT, $CHCl_2$; (b): DEA, THF; (c): EDCI, HOBT, DCM; (d): Tis, TFA, H_2O

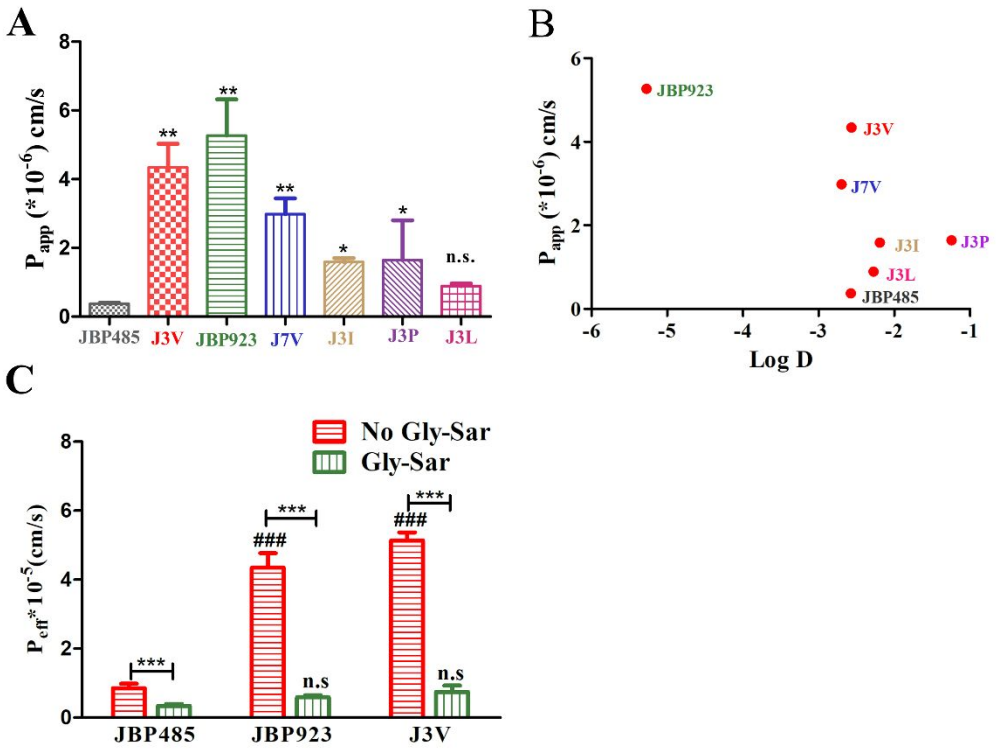

Figure 3. (A) The apparent permeability (P_{app} in cm/s) of JBP485 and its prodrugs at 0.5 mM across Caco-2 monolayers (n=3, technical replicates); *P < 0.05 vs control and **P < 0.01 vs control. The inset P values indicate the significance between groups; (B) The Log D and Caco-2 permeation rate profile of JBP923, JBP485 and its prodrugs (J3V, J3I, J3L and J3P); (C) The permeability coefficient (P_{eff}, cm/s) obtained in situ rat perfusion study for JBP485, J3V and JBP923 at 5 mM (n=3, technical replicates); ***P < 0.005 vs control, ### P < 0.005 vs JBP485 without Gly-Sar, n.s vs JBP485 with Gly-Sar. The inset P values indicate the significance between groups.

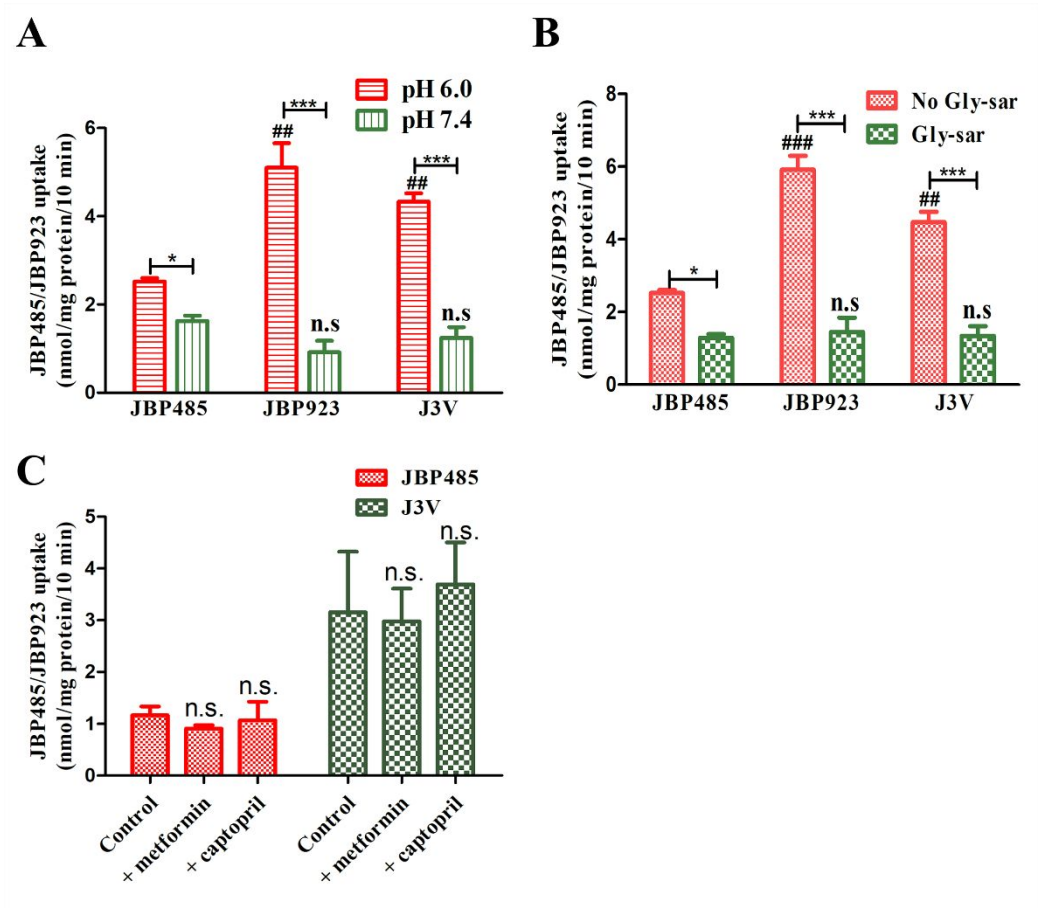

Figure 4. (A) Extracellular pH on the cellular uptake of JBP485, J3V and JBP923 by Caco-2 cells (n=3, technical replicates). *P < 0.05 vs control, **P < 0.01 vs control, **P < 0.005 vs control, ## P < 0.01 vs JBP485 at pH 6.0 HBSS buffer, n.s vs JBP485 at pH 7.4 HBSS buffers. The inset P values indicate the significance between groups; (B) Uptake of JBP485, J3V and JBP923 in the presence and absence of the Gly-sar (50 mM) (n=3, technical replicates). *P < 0.05 vs control, ***P < 0.005 vs control, ## P < 0.01 vs JBP485 without Gly-Sar, ### P < 0.005 vs JBP485 without Gly-Sar, n.s vs JBP485 with Gly-Sar. The inset P values indicate the significance between groups.; (C) Uptake of JBP485, J3V in the presence and absence of the metformin (50 mM) and eaptopril (50 mM) (n=3, technical replicates). n.s vs control. The inset P values indicate the significance between groups.

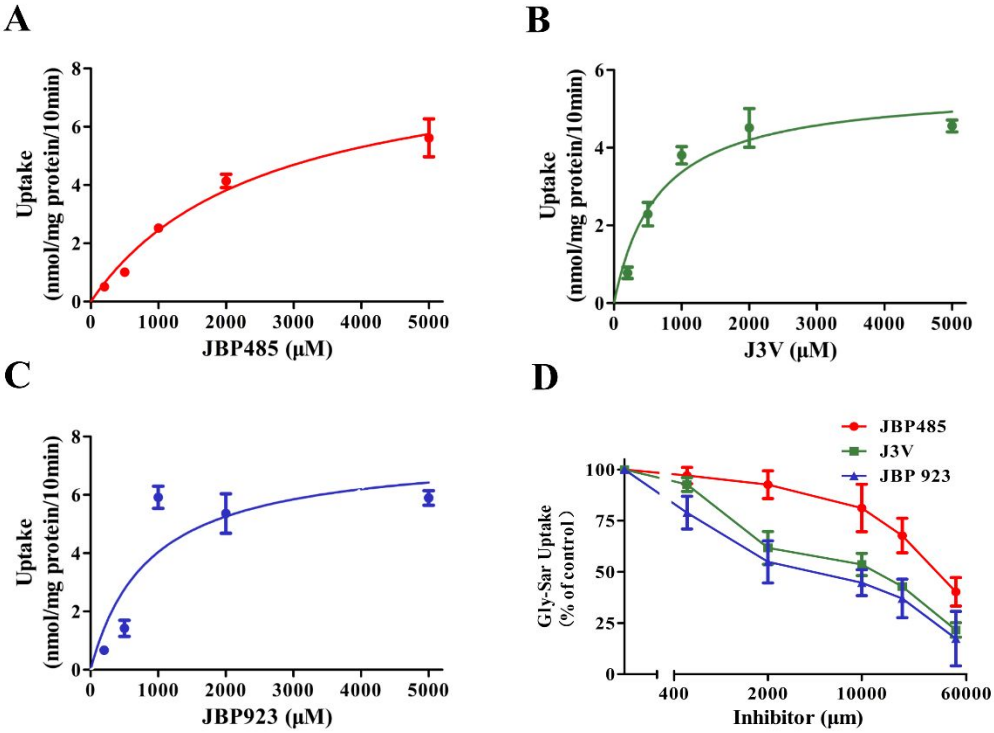

Figure 5. The concentration-dependent uptake of (A) JBP485, (B) J3V, and (C) JBP923 in Caco-2 cells (n=3, technical replicates); (D) Inhibition of JBP485, J3V and JBP923 on the Gly-Sar uptake by Caco-2 cells (n=3, technical replicates).

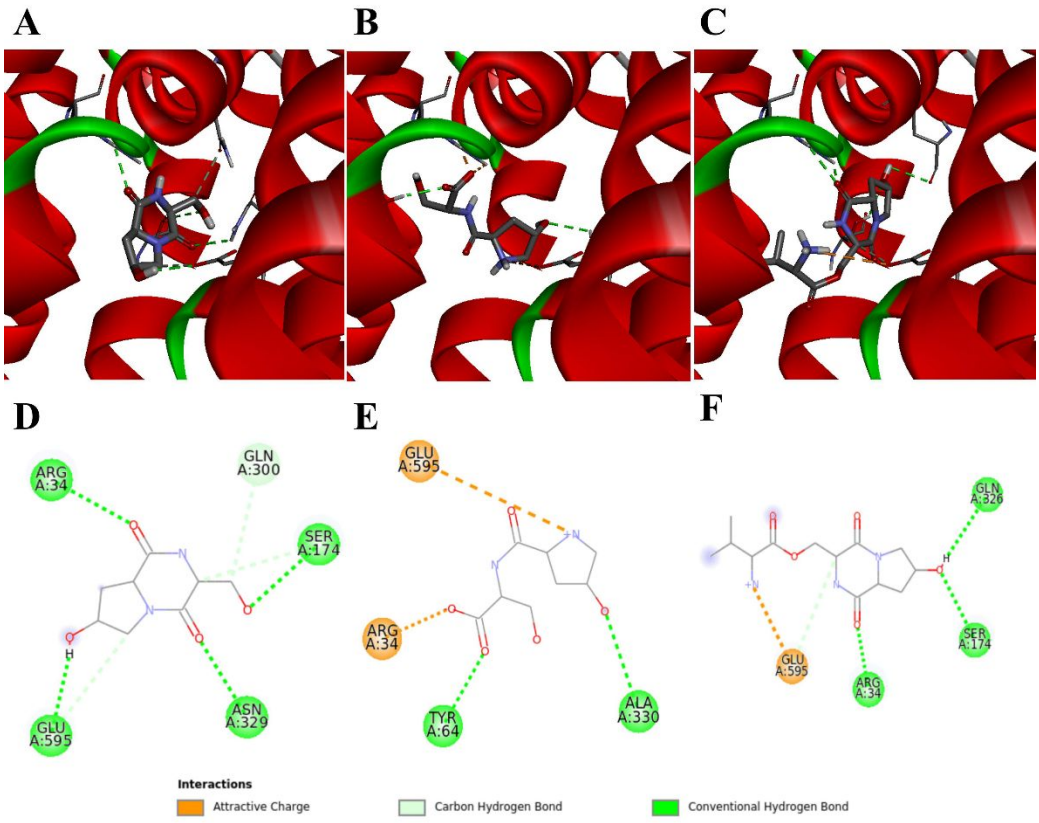

Figure 6. Docking of JBP485 (A, D), JBP923 (B, E) and J3V (C, F) inside the binding site of hPEPT1. The homology model structure of hPEPT1 (with PDB entry 4UVM as the template) was displayed as a solid ribbon colored by secondary structure. The ion-dipole interaction was shown as yellow dotted lines and the weak hydrogen bond interaction was shown as green dotted lines.

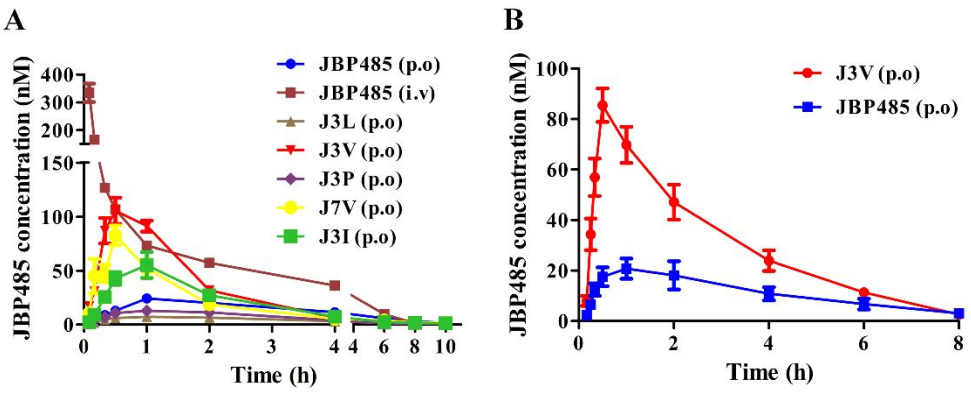

Figure 7. (A) Pharmacokinetic profile in male rats (n=6, technical replicates) of JBP485 after i.v administration of a single 6 mg/kg and oral administration of a single of JBP485, J3V, J3I, J3L, J3P, J7V after oral administration of a single 12 mg/kg dose (calculated as JBP485); (B) Pharmacokinetic profile in male beagle dogs (n=6, technical replicates) of JBP485 and J3V after oral administration of a single 12 mg/kg dose (calculated as JBP485).

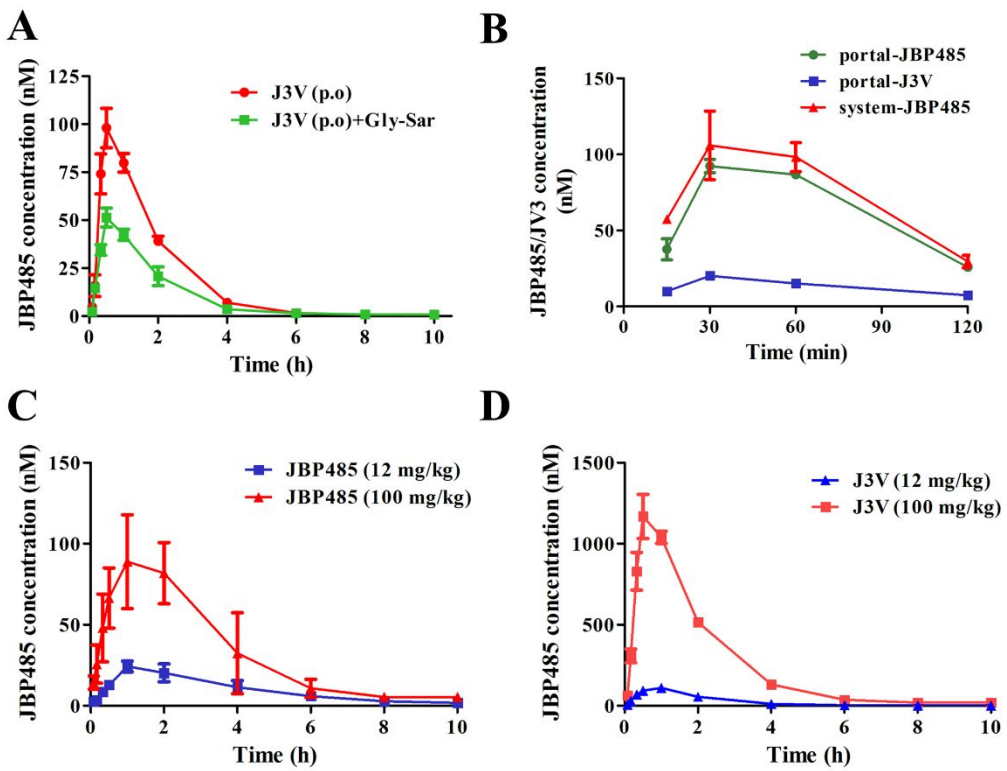

Figure 8. (A) Pharmacokinetic profile of JBP485 after oral administration of J3V (12 mg/kg, calculated as JBP485) to male SD rats in the presence and absence of Gly-Sar (n=6, technical replicates); (B) The hepatic portal and systemic plasma concentration-time profiles of JBP485 and J3V in male SD rats (n=4, technical replicates) after a 12 mg/kg oral administration of J3V (calculated as JBP485); (C, D) Pharmacokinetic profiles of JBP485 after oral administration of JBP485 (12 mg/kg and 100 mg/kg) and J3V (12 mg/kg and 100 mg/kg, calculated as JBP485) to male SD rats (n=6, technical replicates).

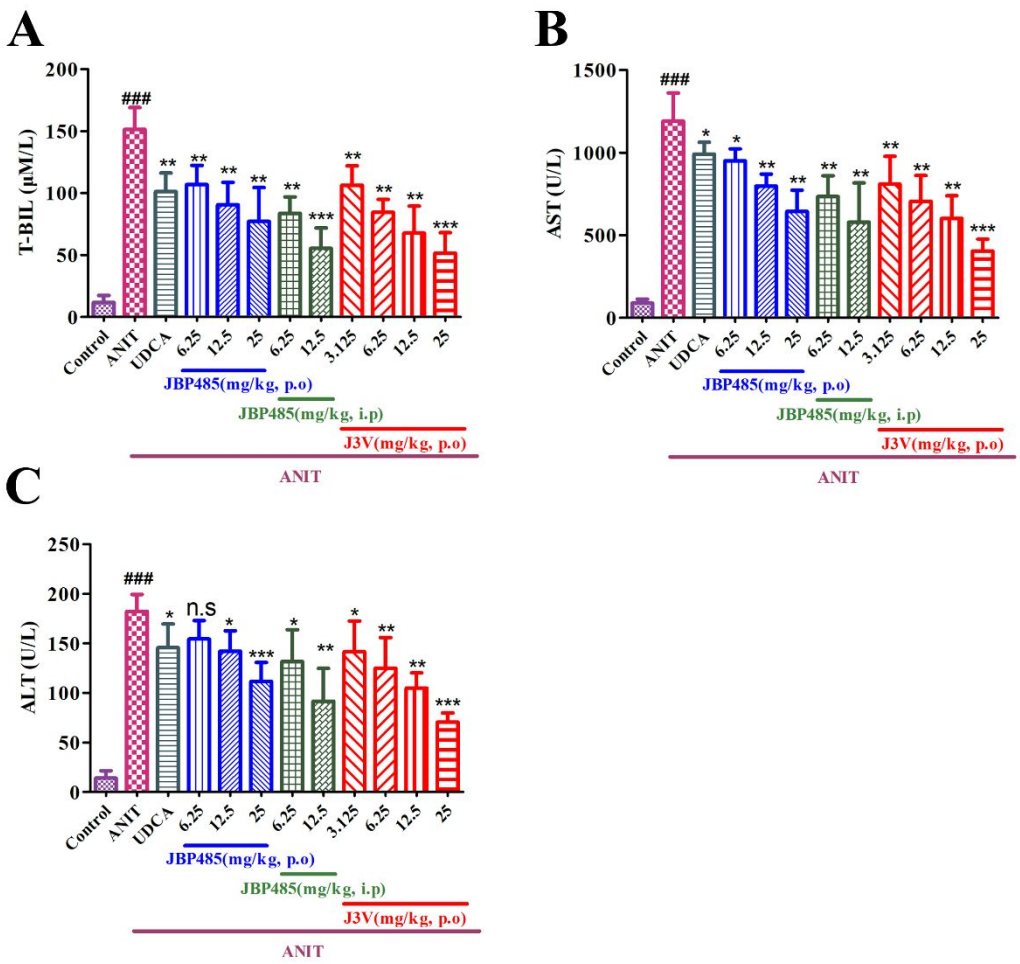

Figure 9. Hepatoprotection of JBP485 and J3V against ANIT-induced hepatotoxicity and cholestasis. Biochemical indicators in male SD rats (n=6, technical replicates) intraperitoneally administered JBP485 (6.25, 12.5 mg/kg) and orally administered vehicle, UDCA (100 mg/kg), JBP485 (6.25, 12.5 and 25 mg/kg) and J3V (3.125, 6.25, 12.5 and 25 mg/kg), respectively, were determined at the time points of 48 h after vehicle or ANIT administration. Serum and T-BIL (A), AST (B), ALT (C) levels elevated by ANIT at 48 h were significantly reduced by treatment with UDCA, different dose of JBP485 and J3V. Data are the mean ± S.D (n = 6, technical replicates), ### $p < 0.005$ vs control and * $P < 0.05$ vs ANIT, ** $P < 0.01$ vs ANIT, *** $P < 0.005$ vs ANIT.

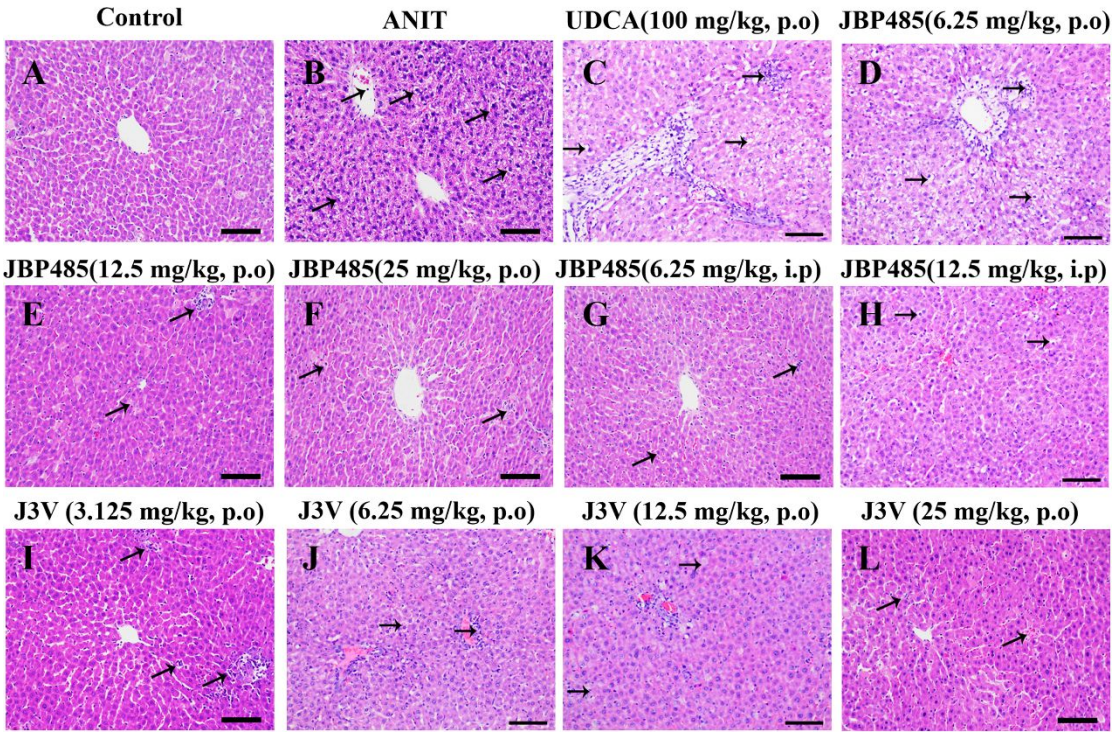

Figure 10. UDCA, JBP485 and J3V attenuated liver injury induced by ANIT in male SD rats. The images of representative H&E stained liver sections (200 ×magnification) at 48 h after ANIT administration were shown. Areas of severe liver necrosis were marked by arrows.

Table of Contents Graphic